The Brucella abortus type IV effector BspA inhibits MARCH6-dependent ERAD to promote intracellular growth

Kambarev, S.; Borghesan, E.; Miller, C.N.; Myeni, S.; Celli, J.

AMERICAN SOCIETY FOR MICROBIOLOGY | Infection and Immunity®

CELLULAR MICROBIOLOGY:
PATHOGEN-HOST CELL MOLECULAR INTERACTIONS

The *Brucella abortus* Type IV Effector BspA Inhibits MARCH6-Dependent ERAD To Promote Intracellular Growth

Stanimir Kambarev,[a] Elizabeth Borghesan,[a] Cheryl N. Miller,[a]* Sebenzile Myeni,[b]§ Jean Celli[a,b,c]

[a]Paul G. Allen School for Global Health, Washington State University, Pullman, Washington, USA
[b]Rocky Mountain Laboratories, National Institute of Allergy and Infectious Diseases, National Institutes of Health, Hamilton, Montana, USA
[c]Department of Microbiology and Molecular Genetics, Larner College of Medicine at the University of Vermont, Burlington, Vermont, USA

ABSTRACT *Brucella abortus*, the intracellular causative agent of brucellosis, relies on type IV secretion system (T4SS) effector-mediated modulation of host cell functions to establish a replicative niche, the *Brucella*-containing vacuole (BCV). *Brucella* exploits the host's endocytic, secretory, and autophagic pathways to modulate the nature and function of its vacuole from an endocytic BCV (eBCV) to an endoplasmic reticulum (ER)-derived replicative BCV (rBCV) to an autophagic egress BCV (aBCV). A role for the host ER-associated degradation pathway (ERAD) in the *B. abortus* intracellular cycle was recently uncovered, as it is enhanced by the T4SS effector BspL to control the timing of aBCV-mediated egress. Here, we show that the T4SS effector BspA also interferes with ERAD, yet to promote *B. abortus* intracellular proliferation. BspA was required for *B. abortus* replication in bone marrow-derived macrophages and interacts with membrane-associated RING-CH-type finger 6 (MARCH6), a host E3 ubiquitin ligase involved in ERAD. Pharmacological inhibition of ERAD and small interfering RNA (siRNA) depletion of MARCH6 did not affect the replication of wild-type *B. abortus* but rescued the replication defect of a *bspA* deletion mutant, while depletion of the ERAD component UbxD8 affected replication of *B. abortus* and rescued the replication defect of the *bspA* mutant. BspA affected the degradation of ERAD substrates and destabilized the MARCH6 E3 ligase complex. Taken together, these findings indicate that BspA inhibits the host ERAD pathway via targeting of MARCH6 to promote *B. abortus* intracellular growth. Our data reveal that targeting ERAD components by type IV effectors emerges as a multifaceted theme in *Brucella* pathogenesis.

KEYWORDS *Brucella*, BspA, ERAD, MARCH6, type IV secretion, endoplasmic reticulum

Bacterial intracellular pathogens utilize sophisticated molecular machineries (type III to type VII secretion systems [T3SS to T7SS, respectively]) to translocate effector proteins into host cells, which modulate diverse cellular processes and promote microbial persistence, proliferation, and dissemination (1). While the effector arsenals of pathogens such as *Salmonella* or *Legionella* have been extensively studied and well characterized, those of other bacteria, such as *Brucella abortus*, remain less understood (1, 2). *B. abortus* is a Gram-negative facultative intracellular pathogen and the causative agent of brucellosis, a global zoonosis with negative impact on both animal and human health (3). Upon infection, the bacterium targets primarily professional phagocytes such as macrophages and dendritic cells, where it undergoes a complex intracellular life cycle. A crucial stage in this process is the VirB T4SS-dependent establishment of a membrane-bound replicative niche, called the *Brucella*-containing vacuole (BCV) (4, 5). This idiosyncratic compartment undergoes a complex maturation during which an initially endosome-like vacuole, called endosomal BCV (eBCV), transitions into an endoplasmic reticulum (ER)-derived, replication-permissive organelle called replicative BCV (rBCV), which supports extensive bacterial proliferation. Finally, the rBCVs are

Editor Andreas J. Bäumler, University of California, Davis

Address correspondence to Jean Celli, jean.celli@med.uvm.edu.

*Present address: Cheryl N. Miller, Pebble Labs, Inc., Los Alamos, New Mexico, USA.

§Present address: Sebenzile Myeni, Department of Medical Microbiology, Leiden University Medical Center, Leiden, The Netherlands.

The authors declare no conflict of interest.

This article is a direct contribution from Jean Celli, a member of the *Infection and Immunity* Editorial Board, who arranged for and secured reviews by Renee Tsolis, University of California, Davis, and Jason Carlyon, Virginia Commonwealth University School of Medicine.

Received 7 April 2023
Accepted 10 April 2023
Published 27 April 2023

converted into autophagosome-like vacuoles called autophagic BCVs (aBCVs), which mediate bacterial egress and reinfection events (6). BCV remodeling relies on T4SS effector-mediated modulation of host cell functions and occurs via sequential interactions with the endocytic, secretory, and autophagic compartments (4, 6, 7). Recently, the ER homeostatic process of protein quality control known as ER-associated degradation (ERAD) was found to be involved in *Brucella* intracellular pathogenesis, via the discovery and characterization of the T4SS effector BspL (8). BspL modulates bacterial egress at the aBCV stage of infection by enhancing ERAD activity through interaction with one of its components, Herp. Whether this host pathway is involved in other aspects of the *Brucella* intracellular cycle is unknown.

ERAD is a multistage cellular process in eukaryotes that maintains ER proteostasis through recognition of both misfolded and functional proteins, their subsequent retrotranslocation through the ER membrane into the cytosol and ubiquitination, and their targeting for proteasomal degradation (9). A key ERAD machinery is the E3 ubiquitin ligase complex, which assembles around a core E3 ubiquitin ligase, an integral transmembrane enzyme that polyubiquitinates targeted ERAD substrates at the ER membrane. More than 25 E3 ubiquitin ligases are associated with the mammalian ER, and at least half of them contribute to one or multiple ERAD branches (9). One such enzyme, MARCH6/TEB4, is a RING-CH domain-containing ubiquitin ligase (10), which together with another ER-resident E3 ligase, HRD1, plays primary roles in ERAD by facilitating the degradation of both luminal and membrane misfolded proteins in mammals. MARCH6 also mediates proteasomal degradation of various properly folded proteins, such as the Hrd1 cofactor FAM8A1, type 2 iodothyronine deiodinase (D2), squalene monooxygenase (SQLE) and perilipin 2 (PLIN2) (11–14), suggesting that MARCH6 is involved in regulating cellular processes other than ER proteostasis, including thyroid hormone homeostasis and lipid metabolism. The composition of the MARCH6 E3 complex is poorly understood. At the mammalian ER membrane, it nucleates additional proteins, such as the cognate ubiquitin-conjugating enzymes (E2s) UBE2J2 and UBE2G2 (9, 10, 15). Based on its homology with the yeast E3 ligase Doa10, MARCH6 supposedly recruits the ATPase p97/VCP through the action of FAF2/UBXD8 (16), a mammalian UBX motif-containing homolog of the yeast protein Ubx2 (17, 18). However, this interaction has not been experimentally confirmed.

While the involvement of the metazoan ERAD machinery in the intracellular lifestyles of many plant pathogens has been well studied (reviewed in reference 19), the relevance of this host pathway for mammalian pathogens is poorly understood. Aside from *Brucella* (8), *Legionella pneumophila* subverts proteasomal degradation for scavenging of amino acids and to regulate the stability of Dot/Icm T4SS effectors in a p97-dependent manner (20, 21) and the causative agent of scrub typhus, *Orientia tsutsugamushi*, temporarily inhibits ERAD to gain access to free amino acids in the cytosol (22). Here, we report that the *B. abortus* VirB T4SS effector BspA inhibits the host ERAD pathway at the rBCV stage of infection through interaction with the ER-resident E3 ubiquitin ligase MARCH6 in order to promote *B. abortus* replication. BspA interferes with the interaction between MARCH6 and its p97/VCP recruitment factor, UBXD8, which subsequently inhibits the MARCH6-dependent axis of the pathway. Altogether, our findings uncover a role of the host ERAD in *B. abortus* intracellular growth and indicate that the T4SS effector-mediated modulation of this pathway emerges as a multifaceted theme in *Brucella* molecular pathogenesis.

RESULTS

BspA is required for *B. abortus* intracellular growth. We originally identified BspA as a *Brucella* VirB T4SS effector translocated into macrophages during infection and that localized to the host ER when ectopically expressed in HeLa cells (23). Yet, whether BspA contributes to *Brucella* intracellular pathogenesis was not clearly established. To gain further insight into BspA's function, we first investigated its requirement for *Brucella* intracellular growth in a bone marrow-derived murine macrophage (BMM) infection model. A hallmark of *Brucella* intracellular trafficking is the progressive exclusion of endosomal

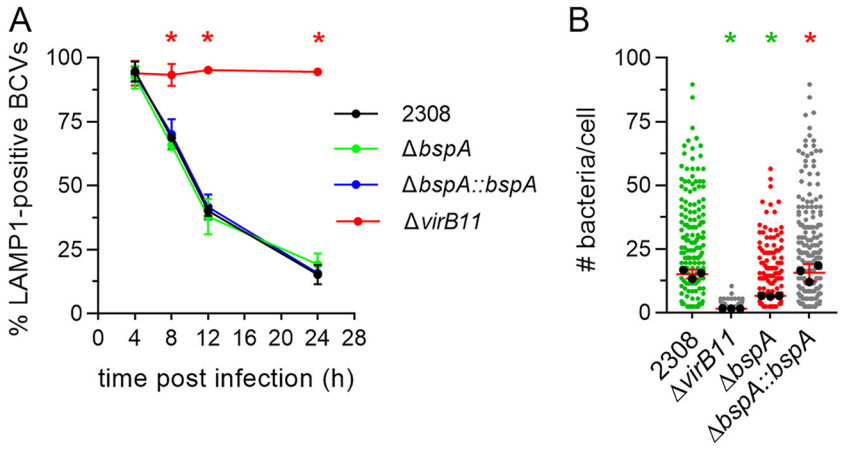

FIG 1 BspA is required for *Brucella* intracellular growth. (A) LAMP1 exclusion assay as a readout for eBCV-to-rBCV transition. BMMs were infected with either the wild-type (2308), Δ*virB11* mutant, Δ*bspA* mutant, or Δ*bspA* complemented (Δ*bspA*::*bspA*) *B. abortus* strain, and rBCV biogenesis was evaluated by scoring LAMP1-positive BCVs over a 24-h period. Data represent means ± SD from at least three independent experiments, and statistical significance between conditions is indicated with asterisks ($P < 0.05$, as determined by two-way ANOVA, followed by Dunnett's multiple-comparison test against 2308 as a control). (B) Intracellular replication assay in macrophages. BMMs were infected with either the wild-type (2308), Δ*virB11* mutant, Δ*bspA* mutant, or Δ*bspA* complemented (Δ*bspA*::*bspA*) *B. abortus* strain, and intracellular bacterial loads were scored at 24 hpi by enumeration of bacteria per infected cell ($n > 300$). Data represent means ± SD from at least three independent experiments, and statistical significance is indicated with color-coded asterisks ($P < 0.05$, as determined by one-way ANOVA followed by Dunnett's multiple-comparison test using 2308 [green] or the Δ*bspA* mutant [red] as comparisons).

markers from its early eBCV, a process that is T4SS dependent and leads to biogenesis of the replication-permissive rBCV (4, 5, 7, 24–27). BMMs infected with either wild-type *B. abortus* 2308, a Δ*virB11* T4SS-deficient mutant, an in-frame Δ*bspA* deletion mutant (23), or its chromosomally complemented Δ*bspA*::*bspA* strain were analyzed by fluorescence microscopy for exclusion of the LAMP1 late endosome/lysosomal marker from BCVs over a 24-h period (Fig. 1A). Compared to Δ*virB11* bacteria that failed to undergo eBCV-to-rBCV transition (4, 5), wild-type, Δ*bspA*, and Δ*bspA*::*bspA* bacteria displayed similar kinetics of LAMP1 exclusion (Fig. 1A), indicating that BspA is not required for rBCV biogenesis. However, when bacterial replication was quantified in individual BMMs at 24 h postinfection (hpi), both the Δ*virB11* and Δ*bspA* mutants showed significantly lower replication levels than the wild-type *B. abortus* ($P < 0.0001$ and $P = 0013$, respectively) (Fig. 1B). The growth defect of the Δ*bspA* mutant was rescued by genetic complementation with a single chromosomal copy of *bspA* (the Δ*bspA*::*bspA* strain; $P = 0.0009$). Taken together, these findings indicate that BspA contributes to *B. abortus* intracellular growth within rBCVs but not rBCV biogenesis.

BspA interacts with the host E3 ubiquitin ligase MARCH6. To gain insight into BspA's mode of action, we next sought to identify its host molecular targets. Using a yeast two-hybrid approach, a human monocyte cDNA library was screened against BspA and uncovered BspA interaction with a fragment (residues 166 to 325) of MARCH6/TEB4, a MARCH-family, ER-resident RING-finger E3 ubiquitin ligase involved in the ER-associated degradation (ERAD) pathway (9, 10). This interaction was confirmed by mating the original BspA-expressing yeast strain with yeast strains transformed either with the original $MARCH6_{166–325}$-expressing pGADT7 vector retrieved from the library screen or with a pGADT7 vector expressing full-length $MARCH6_{full}$ (Fig. 2A). These findings were further corroborated by reciprocal coimmunoprecipitation of myc-tagged MARCH6 and 3×FLAG-tagged BspA in HeLa cells (Fig. 2B), and by myc-MARCH6 and 3×FLAG-BspA colocalization at the ER membranes in HeLa cells (Fig. 2C). Hence, BspA directly interacts with the ER-associated protein MARCH6, suggesting that BspA functionally targets the host ERAD pathway.

Inhibition of ERAD is required for BspA-dependent intracellular growth. The replication defect of the Δ*bspA* mutant in BMMs (Fig. 1B) and the interaction of BspA

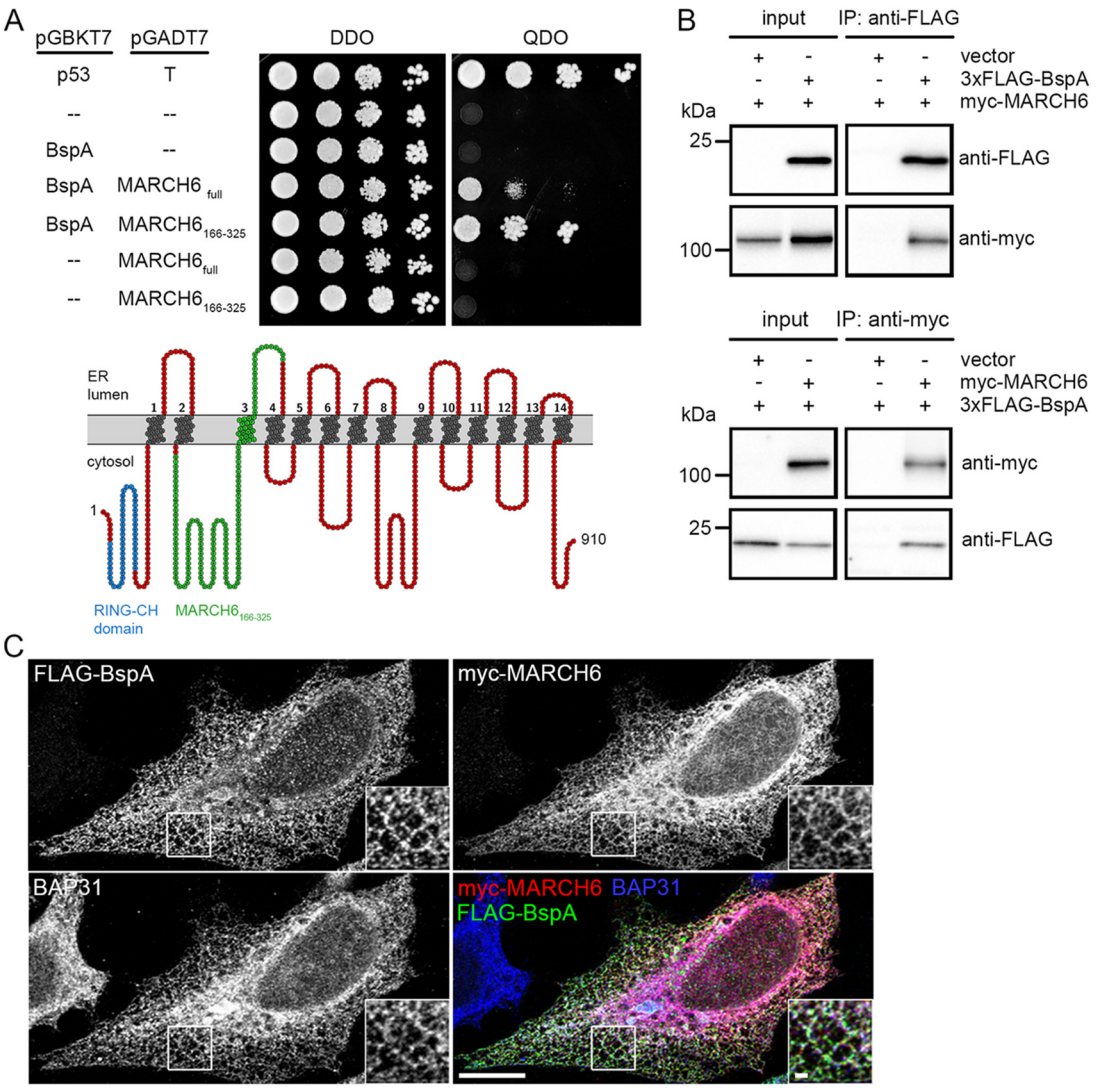

FIG 2 BspA interacts with the host E3 ubiquitin ligase MARCH6. (A) Representative image of the yeast two-hybrid screen showing interaction of BspA with either a 159-amino-acid fragment (residues 166 to 325) of MARCH6 or the full-length protein. Mating between p53- and T-antigen-expressing yeasts served as a positive control, and mating between strains containing empty pGBKT7 and pGADT7 vectors was used for negative controls. The region of interaction ($MARCH6_{166–325}$) is highlighted in blue on the MARCH6 topology model. (B) Coimmunoprecipitation of BspA and MARCH6 in mammalian cells. HeLa cells were cotransfected to produce either 3×FLAG-tagged BspA and myc-tagged MARCH6 or each protein individually, and either 3×FLAG-BspA (upper panel) or myc-MARCH6 (lower panel) was immunoprecipitated using paramagnetic anti-FLAG or anti-myc antibody conjugates. Input samples (1.25% of postnuclear supernatants) and immunoprecipitates were resolved by SDS-PAGE and probed for 3×FLAG-BspA and myc-MARCH6 by Western blotting. (C) Representative confocal micrographs showing colocalization of myc-MARCH6 and 3×FLAG-BspA at the ER. HeLa cells were cotransfected with plasmids expressing 3×FLAG-BspA and myc-MARCH6 for 24 h and processed for immunofluorescence microscopy. BAP31 staining was used to label ER membranes. Scale bars, 10 μm and 1 μm (inset).

with a key component of the mammalian ERAD (Fig. 2) suggested that modulation of this host pathway contributes to *B. abortus* intracellular growth. To test this hypothesis, we inhibited ERAD using kifunensine, an inhibitor of the early ERAD protein α-1,2-mannosidase 1 (EDEM1), which blocks deglycosylation of misfolded ERAD substrates in the ER lumen prior to their retrotranslocation and targeting for proteasomal degradation (28) (Fig. 3A). To verify the effect of kifunensine on ERAD, BMMs were transduced to express the general ERAD substrate, a hemagglutinin (HA)-tagged "null Hong Kong" mutant variant of human α-1-antitrypsin (NHK) (9, 29, 30). Kifunensine treatment of BMMs increased the steady-state level of NHK, indicating ERAD inhibition ($P = 0.0287$) (Fig. 3B). In BMMs treated with 1.5 μM kifunensine between 2 and 24 hpi, wild-type *B. abortus* showed similar replication efficiency to mock-treated BMMs (Fig. 3C),

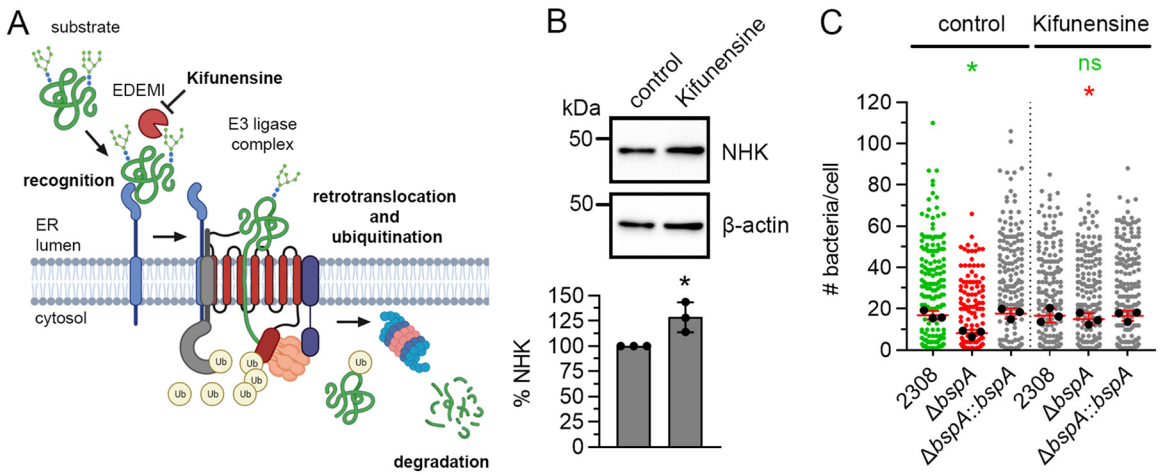

FIG 3 ERAD inhibition restores BspA-dependent intracellular replication of *Brucella*. (A) Model of the mammalian ERAD pathway. A misfolded ERAD substrate is first recognized in the ER lumen and then recruited to the E3 ubiquitin ligase complex at the ER membrane. The misfolded protein is retrotranslocated trough the ER membrane and concomitantly ubiquitinated by the concerted action of the E3 ubiquitin ligase and the p97/VCP ATPase. The retrotranslocated substrate is degraded by the proteasome in the cytosol. Kifunensine is an ERAD inhibitor that targets the deglycosylation enzyme EDEM1. Created using BioRender (www.biorender.com). (B) Representative immunoblots of ERAD inhibition by kifunensine. BMMs were seeded in 6-well plates at a density of 3×10^5 cells/well and retrovirally transduced to express HA-tagged NHK at 24 h postseeding. The samples were then treated as for a 24-h infection, collected in 2× SDS-PAGE sample buffer, and resolved by SDS-PAGE. The lysates were probed for NHK-HA by Western blotting, and the steady-state levels of the substrate were quantified by densitometry analysis. Data represent means ± SD from at least three independent experiments, and statistical significance is indicated with asterisks ($P = 0.0287$, as determined with unpaired, two-tailed Student's *t* test against nontreated controls). (C) Effect of kifunensine on *Brucella* intracellular replication. BMMs were infected with either the wild-type (2308), Δ*bspA* mutant, or Δ*bspA* complemented (Δ*bspA*::*bspA*) *B. abortus* strain and treated with 1.5 μM kifunensine at 2 hpi to avoid interference with bacterial uptake. At 24 hpi, samples were fixed and analyzed by enumeration of bacteria per infected cell ($n > 300$). Data represent means ±SD from at least three independent experiments, and statistical significance is indicated with asterisks ($P = 0.0020$ and 0.0107, as determined by two-way ANOVA, followed by Dunnett's multiple-comparison test against 2308 and the Δ*bspA* strain as controls, respectively).

suggesting that impairment of ERAD does not affect *B. abortus* intracellular replication capacity. In contrast, kifunensine treatment restored replication of Δ*bspA* bacteria ($P = 0.0107$) to levels observed for wild-type or Δ*bspA*::*bspA* complemented bacteria (Fig. 3C). This indicates that inhibition of ERAD suppresses the growth defect caused by deletion of *bspA*, suggesting that BspA interferes with ERAD to promote *B. abortus* intracellular growth.

BspA-dependent replication of *B. abortus* requires inhibition of MARCH6-dependent ERAD. Due to its upstream target along the multistep ERAD pathway, Kifunensine did not specifically inform the functional contribution of downstream ERAD stages such as ubiquitination and retrotranslocation (Fig. 3A) to BspA-dependent replication of *B. abortus*. We therefore decided to modulate the pathway in a targeted manner by specifically depleting different ERAD components, namely, the E3 ubiquitin ligases March6 and Hrd1 and the ERAD adapter Ubxd8 (Fig. 4A), via small interfering RNA (siRNA)-mediated silencing (Fig. 4B and C). Hrd1 is another ER-resident RING finger E3 ubiquitin ligase involved in ERAD, which has a primary role in ubiquitination of ER luminal and ER membrane substrates (9, 31). Ubxd8 is a UBX-motif containing protein that functions downstream of the E3 ligase complex and recruits the ATPase p97/VCP to the E3 complex, thus facilitating the retrotranslocation of ubiquitinated substrates through the ER membrane (9, 16). While depletions of Hrd1 and Ubxd8 were assessed via Western blotting, that of March6 was assessed via quantitative reverse transcription-PCR (RT-qPCR) as no specific anti-March6 antibodies were found to be specific (Fig. 4B and C). To control whether depletion of these ERAD components affected ERAD activity, BMMs were treated with either nontargeting, March6-, Hrd1- or Ubxd8-specific siRNAs for 72 h and transduced for 48 h to express either NHK-HA or the March6-dependent C-terminally 3×FLAG-tagged ERAD substrate, type 2 iodothyronine deiodinase (D2-3×FLAG) (12), and their steady-state levels were measured. The level of NHK-HA significantly increased only in cells depleted of Hrd1 ($P = 0.016$) (Fig. 4D)

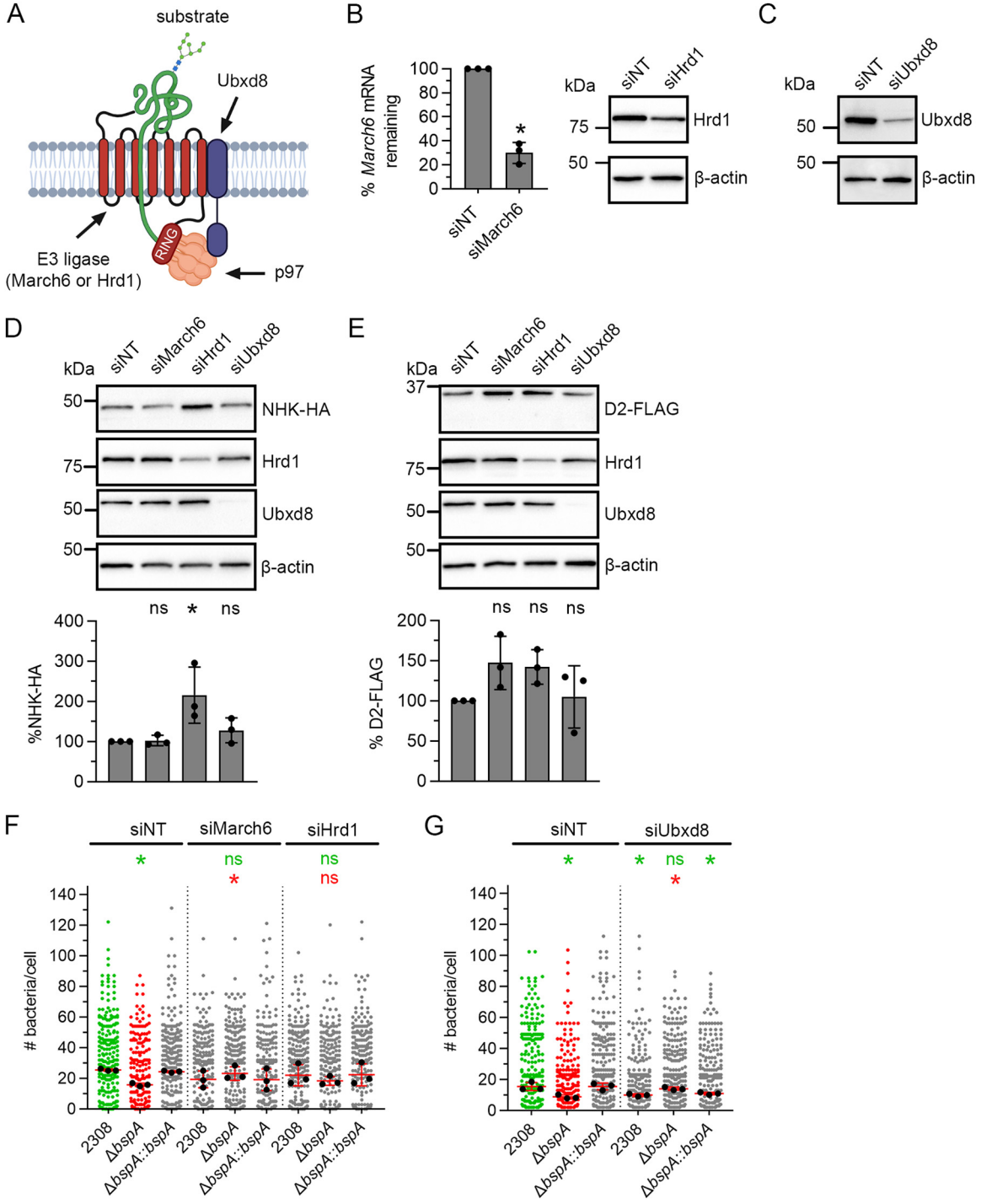

FIG 4 BspA-dependent replication of *Brucella* requires inhibition of MARCH6-dependent ERAD. (A) Model of the ERAD E3 ubiquitin ligase complex at the ER membrane. The complex nucleates around a core E3 ubiquitin ligase, which retrotranslocates and ubiquitinates the targeted substrate via its catalytic RING domain. Subsequently, the Ubx-motif-containing protein Ubxd8 recruits the ATPase p97 to the E3 complex that provides energy for the retrotranslocation of the substrate through the ER membrane. Created using BioRender (www.biorender.com). (B and C) Representative depletion of March6, Hrd1, and Ubxd8 in siRNA-treated BMMs compared to nontargeting (siNT) controls. Depletion of endogenous March6 was assessed via RT-qPCR as no specific anti-March6 antibodies were found for Western blotting. Relative levels of *March6* mRNA were quantified using *March6*-specific primers. Primers specific for mouse ribosomal *rplp0* were used for normalization. Data represent means ± SD from at least three independent experiments, and statistical significance is indicated with asterisks (69.95% ± 5.063% depletion; $P = 0.0002$, as determined with unpaired, two-tailed Student's *t* test against nontargeting control). Depletion of Hrd1 and Ubxd8 was monitored and quantified by Western blotting (63.64% ± 6.735% and 88.05% ± 0.3283% depletion; $P = 0.0007$ and 0.0001, respectively, as determined with unpaired, two-tailed Student's *t* test against nontargeting control), where probing for *β*-actin served as loading control. (D and E)

(Continued on next page)

compared to nontargeting controls, while that of D2-3×FLAG increased upon siRNA silencing of either March6 or Hrd1 (Fig. 4E), although statistical significance was not achieved. Depletion of Ubxd8 did not alter NHK-HA steady-state levels (Fig. 4D and E). Analysis of bacterial replication in BMMs treated with either siNT (a nontargeting control siRNA), siMarch6, siHrd1, or siUbxd8 siRNAs and infected with either wild-type *B. abortus*, Δ*bspA*, or Δ*bspA*::*bspA* bacteria for 24 h showed that depletions of neither March6 nor Hrd1 (depletions of 70.0% ± 5.1% and 63.6% ± 6.7%, respectively) (Fig. 4B and C) affected replication of wild-type bacteria (Fig. 4F), consistent with the effect of kifunensine (Fig. 3C). Depletion of Ubxd8 (88.0% ± 0.3%) (Fig. 4C) decreased replication of wild-type bacteria and the complemented Δ*bspA*::*bspA* strain ($P = 0.0054$ and 0.0193, respectively) (Fig. 4G), suggesting that Ubxd8 functions contribute to *B. abortus* replication. Interestingly, depletions of either March6 or Ubxd8 significantly rescued the replication defect of the Δ*bspA* deletion mutant ($P = 0.0485$ in panel F and $P = 0.0015$ in panel G), phenocopying the effect of kifunensine on the Δ*bspA* deletion mutant (Fig. 3C). In contrast, depletion of Hrd1 only partially rescued replication of Δ*bspA* bacteria, with no statistically significant differences achieved compared to either wild-type or Δ*bspA* bacteria in siNT-treated BMMs (Fig. 4F), suggesting that Hrd1-mediated ERAD is not the ERAD pathway targeted by BspA. Collectively, these results can be interpreted as indicating that BspA-dependent replication of *B. abortus* predominantly requires inhibition of MARCH6-dependent ERAD and Ubxd8.

***B. abortus* inhibits ERAD at the rBCV stage in a BspA-dependent manner.** To test whether BspA interferes with ERAD activity during infection, BMMs were transduced to express the ERAD substrate NHK-HA and mock infected or infected with either wild-type or Δ*bspA B. abortus* strains for 24 h, after which steady-state levels of NHK-HA were examined by Western blotting. Compared to mock-infected BMMs, infections with either wild-type or Δ*bspA* bacteria caused an increase in NHK-HA steady-state levels that was significant only for wild-type bacteria ($P = 0.0113$) and no significant differences in NHK-HA levels could be observed between infections with wild-type and Δ*bspA* bacteria (Fig. 5A), possibly due to the broad variability of our results among the 7 independent experiments performed (Fig. 5A). As this approach did not provide compelling evidence that *B. abortus* altered ERAD activity in a BspA-dependent manner, we next sought direct evidence of BspA's effect on ERAD activity and tested whether ectopic expression of 3×FLAG-BspA in BMMs alters the steady-state levels of various ERAD substrates. BMMs were cotransduced to express either NHK-HA or D2-3×FLAG, with or without 3×FLAG-BspA, and steady-state levels of either NHK-HA or D2-3×FLAG were examined by Western blotting. Compared to vector control conditions, BspA production in BMMs led to a significant increase in both NHK-HA ($P = 0.0353$) and D2 ($P = 0.0228$) (Fig. 5), indicating that BspA is sufficient to inhibit ERAD activity.

Although commonly accepted as a readout for ERAD activity, steady-state levels of ERAD substrates can be confounded by changes in expression levels and do not necessarily reflect only changes in stability. We therefore used an alternative, fluorescence microscopy-based assay of ERAD substrate retrotranslocation in the cytosol, which takes advantage of the deglycosylation-dependent (dd) substrate NHK-ddVenus (32). This modified ERAD substrate adopts its native state and emits a fluorescent signal

FIG 4 Legend (Continued)
Representative immunoblots showing the effect of March6, Hrd1, and Ubxd8 depletion on the steady-state levels of NHK-HA and D2-3×FLAG in BMMs, respectively. Graphs represent the relative levels of the two substrates in BMMs treated with either nontargeting (siNT) siRNA or siRNAs specific for March6, Hrd1, and Ubxd8 and subsequently retrovirally transduced to express either NHK-HA or D2-3×FLAG. The levels of the two substrates were determined by Western blotting and densitometry, in which β-actin served as the loading control. Data represent means ± SD from at least three independent experiments, and statistical significance is indicated with asterisks ($P = 0.0160$, as determined by one-way ANOVA, followed by Dunnett's multiple comparison against siNT as a control). (F and G) siRNA-mediated depletion of March6 and Ubxd8 but not Hrd1 restores BspA-dependent replication of *Brucella*. BMMs were nucleofected with either nontargeting siRNA (siNT) or siRNAs against March6, Ubxd8, or Hrd1 and then infected with either the wild-type (2308), Δ*bspA* mutant, or Δ*bspA* complemented (Δ*bspA*::*bspA*) *B. abortus* strain. At 24 hpi, samples were fixed and the numbers of bacteria per infected cell ($n > 300$) were enumerated. Data represent means ± SD from at least three independent experiments, and statistical significance is indicated with asterisks ($P = 0.0001$ and 0.0485 in panel F and $P = 0.0015$ in panel G, as determined by two-way ANOVA, followed by Dunnett's multiple-comparison test with 2308/siNT or Δ*bspA*/siNT as the control).

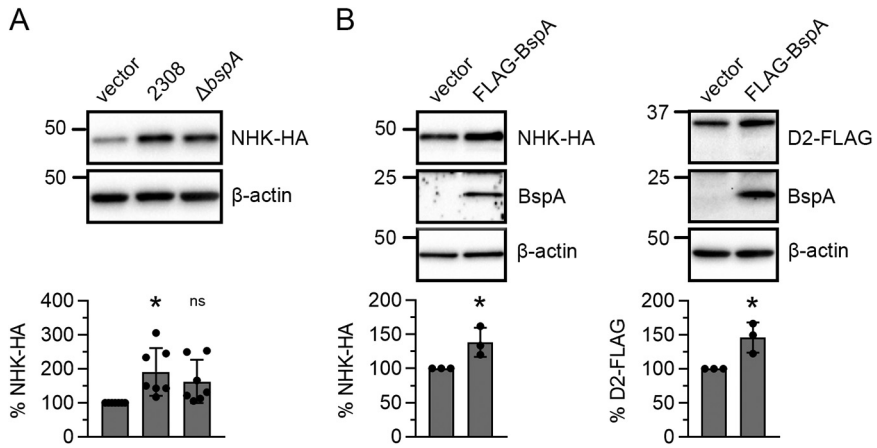

FIG 5 BspA inhibits host ERAD. (A) Effect of *Brucella* infection on the steady-state levels of NHK-HA in macrophages. BMMs were transduced to express NHK-HA for 48 h and then either mock infected or infected with the wild-type 2308 or Δ*bspA* mutant *B. abortus* strain for 24 h at an MOI of 1,000. Samples were collected at 24 hpi, and the steady-state level of NHK-HA was quantified by Western blotting against β-actin levels as the loading control. Data represent means ± SD from seven independent experiments, and statistical significance is indicated with asterisks (P = 0.0113, as determined by one-way ANOVA, followed by Dunnett's multiple-comparison test with mock-infected samples). (B) Effect of ectopically expressed 3×FLAG-BspA on the steady-state levels of NHK-HA and D2-3×FLAG in macrophages. BMMs were cotransduced for 72 h to express either NHK-HA or D2-3×FLAG, with or without 3×FLAG-BspA, and samples were analyzed by quantitative Western blotting using β-actin levels as the loading control. Data represent means ± SD from at least three independent experiments, and statistical significance is indicated with asterisks (P = 0.0228 and P = 0.0353, respectively, determined with unpaired, two-tailed Student's t test against empty vector controls).

only after it has been retrotranslocated through the ER membrane via ERAD and deglycosylated in the cytosol (Fig. 6A). In support of this approach, a similar ddVenus-based assay was recently used to show that the *B. abortus* T4SS effector BspL modulates ERAD activity to regulate the timing of bacterial egress at the aBCV stage of infection (8). As we could not detect NHK-ddVenus production or fluorescence via retroviral transduction of BMMs, we alternatively used HeLa cells, an established, surrogate model of *Brucella* infection (5–7, 33, 34), where transient transfection produced detectable NHK-ddVenus (Fig. 6B). We first cotransfected HeLa cells with NHK-ddVenus and either pmCherry (as an irrelevant protein control) or pCMV-3×FLAG-BspA for 24 h and then treated the cells with the proteasome inhibitor MG132 for 3 h to allow for NHK-ddVenus fluorescence accumulation in the cytosol and quantified NHK-ddVenus fluorescence intensities by microscopy image analysis. Consistent with our findings in BMMs that BspA increases steady-state levels of the ERAD substrate NHK or D2 (Fig. 5), HeLa cells expressing 3×FLAG-BspA showed significantly lower NHK-ddVenus signal than the one expressing mCherry (P = 0.0064), indicating a reduced retrotranslocation of ERAD substrates resulting from impaired ERAD function (Fig. 6C). Taken together, these results confirm that ectopically expressed BspA inhibits the host ERAD pathway.

We next took advantage of the NHK-ddVenus assay to test whether BspA inhibits ERAD during infection. HeLa cells were mock infected or infected with either the wild-type, Δ*bspA* mutant, or Δ*bspA*::*bspA* complemented *B. abortus* strain, transfected to express NHK-ddVenus at 2 hpi, treated with MG132 at 21 hpi, and processed for NHK-ddVenus fluorescence image analysis at 24 hpi. Infection with wild-type bacteria caused a significant decrease in NHK-ddVenus cytosolic signal ($P < 0.0001$) (Fig. 6D and E), indicating that ERAD activity is impaired upon infection at 24 hpi. Infection with Δ*bspA* bacteria also caused a significantly reduced NHK-ddVenus cytosolic signal (P = 0.0005) (Fig. 6D and E) compared to uninfected cells, which was also significantly higher than that caused by infection with wild-type bacteria (P = 0.0014) (Fig. 6E). Genetic complementation of the Δ*bspA* mutant restored NHK-ddVenus signal to the level induced by wild-type bacteria (Fig. 6D and E), confirming that the phenotypic

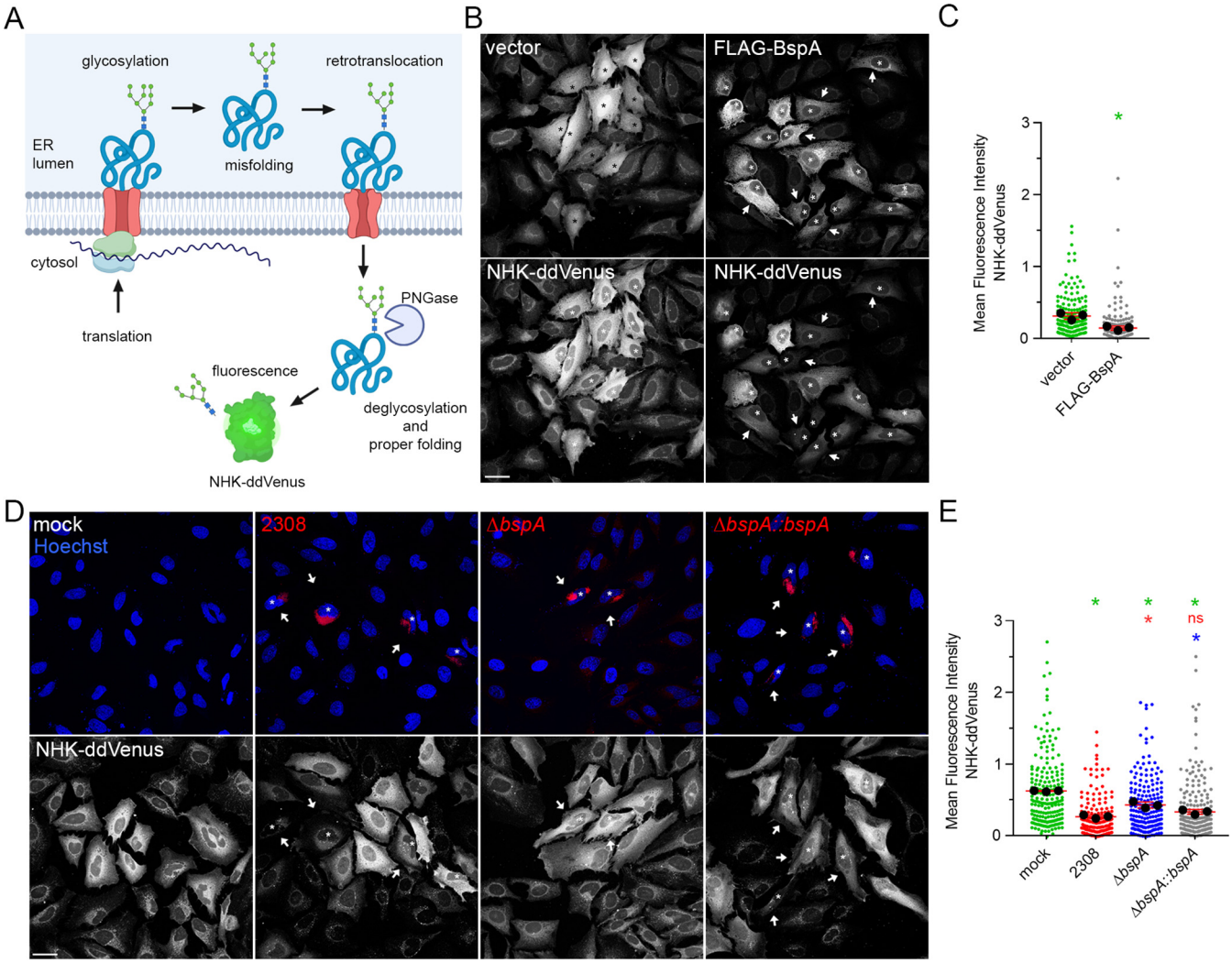

FIG 6 *Brucella* inhibits ERAD at the rBCV stage in a BspA-dependent manner. (A) Schematic representation of the deglycosylation-dependent fluorescence of NHK-ddVenus. The translated NHK-ddVenus polypeptide is glycosylated in the ER, which leads to aberrant folding and lack of fluorescence. The misfolded protein is then recognized by the ERAD pathway and retrotranslocated into the cytosol. Retrotranslocated NHK-ddVenus is deglycosylated by the cytosolic peptide:N′ glycanase (PNGase) and adopts its native, fluorescent conformation. Created using BioRender (www.biorender.com). (Based on data from reference 32.) (B) Representative confocal micrographs showing NHK-ddVenus fluorescence in HeLa cells expressing either mCherry (control) or 3×FLAG-BspA. Asterisks indicate cotransfected cells; arrowheads indicate 3×FLAG-BspA-producing cells in which NHK-ddVenus is decreased. Scale bars, 10 μm. (C) Effect of ectopically expressed 3×FLAG-BspA on the relative fluorescence intensity of NHK-ddVenus. HeLa cells were cotransfected to express NHK-ddVenus with either mCherry or 3×FLAG-BspA for 24 h. At 21 h posttransfection, cells were treated for 3 h with 20 μM MG132. At 24 h posttransfection, samples were processed for immunostaining and whole cells were imaged by fluorescence microscopy. NHK-ddVenus fluorescence intensity was measured using Fiji ImageJ. Data represent means ± SD from at least three independent experiments, and statistical significance is indicated with asterisks ($P = 0.0064$, as determined by unpaired, two-tailed Student's *t* test against the mCherry vector control). (D) Representative confocal micrographs of NHK-ddVenus fluorescence in *Brucella*-infected HeLa cells. HeLa cells were either mock infected or infected with the wild-type (2308), Δ*bspA* mutant, or Δ*bspA* complemented (Δ*bspA*::*bspA*) *B. abortus* strain for 24 h. Infected cells were transfected to produce NHK-ddVenus at 2 hpi, and cells were treated at 21 hpi for 3 h with 20 μM MG132. Asterisks indicate infected cells; arrowheads indicate infected cells in which NHK-ddVenus is decreased. Scale bars, 10 μm. (E) Effect of *Brucella* infection on NHK-ddVenus fluorescence intensity. HeLa cells were either mock infected or infected with the wild-type (2308), Δ*bspA* mutant, or Δ*bspA* complemented (Δ*bspA*::*bspA*) *B. abortus* strain for 24 h. Infected cells were transfected to produce NHK-ddVenus at 2 hpi, and cells were treated at 21 hpi for 3 h with 20 μM MG132. NHK-ddVenus quantitative fluorescence analysis was performed as in panel C. Data represent means ± SD from at least three independent experiments, and statistical significance is indicated by asterisks ($P < 0.05$, as determined by one-way ANOVA, followed by Dunnett's multiple-comparison test with mock-infected samples).

defect observed was BspA dependent. Hence, these results demonstrate that *B. abortus* inhibits ERAD during the rBCV stage and that this inhibition is partially mediated by BspA.

BspA inhibits the host MARCH6-dependent ERAD though disruption of the MARCH6-UbxD8 interaction. Having established the contribution of BspA to ERAD inhibition during *B. abortus* infection, we next investigated the mode of action of BspA, based on its interaction with March6 (Fig. 2) and its functional relationship with

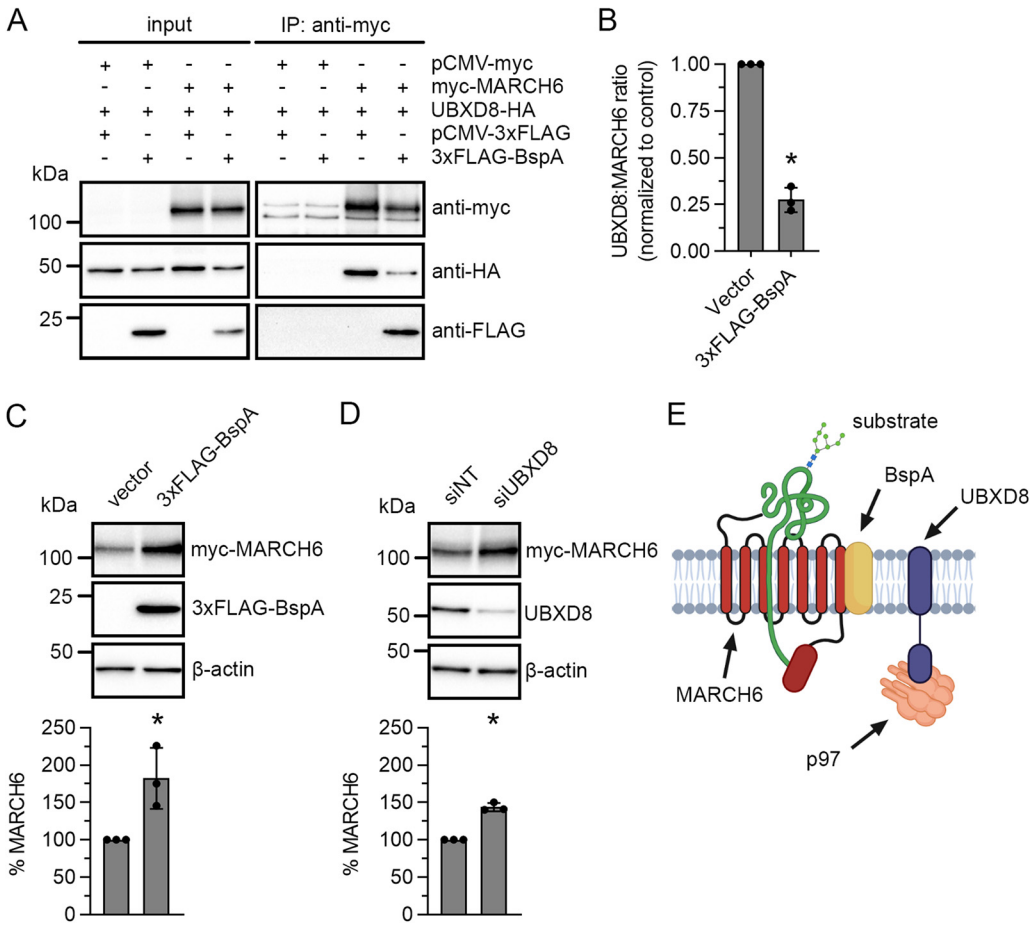

FIG 7 BspA disrupts the MARCH6-UBXD8 interaction in HeLa cells. (A and B) Representative immunoblots showing the effect of BspA on the coimmunoprecipitation of UBXD8 with MARCH6. HeLa cells were cotransfected for 24 h to produce myc-MARCH6 and UBXD8-HA in the presence or absence of 3×FLAG-BspA, followed by cross-linking and immunoprecipitation of myc-MARCH6 using paramagnetic anti-myc antibody conjugates. Inputs (1.25% of postnuclear supernatants) and immunoprecipitates were resolved by SDS-PAGE and probed for myc-MARCH6, UBXD8-HA, and 3×FLAG-BspA by Western blotting. The UBXD8/MARCH6 ratio was quantified by densitometric analysis. Data represent means ± SD from at least three independent experiments, and statistical significance is indicated by asterisks ($P < 0.0001$, as determined by unpaired, two-tailed Student's *t* test against the empty vector control). (C) Representative immunoblots showing the effect of 3×FLAG-BspA on the steady-state level of myc-MARCH6. HeLa cells were cotransfected to coexpress myc-MARCH6 with 3×FLAG-BspA or not (vector). Samples were collected at 24 h posttransfection and resolved by SDS-PAGE. myc-MARCH6 levels were determined by quantitative Western blotting against β-actin as the loading control. Data represent means ± SD from at least three independent experiments, and statistical significance is indicated with asterisks ($P = 0.0252$, as determined by unpaired, two-tailed Student's *t* test against the empty vector control). (D) Representative Western blots showing the effect of siRNA-mediated depletion of UBXD8 (71.95% ± 9.262%) on the steady-state level of myc-MARCH6. HeLa cells were transfected with either nontargeting (siNT) or UBXD8-specific siRNAs (siUBXD8) for 48 h. At 24 h posttransfection, cells were transfected to produce myc-MARCH6 for 24 h. Samples were collected and resolved by SDS-PAGE. myc-MARCH6 levels were determined by quantitative Western blotting against β-actin as the loading control. Data represent means ± SD from at least three independent experiments, and statistical significance is indicated with asterisks ($P = 0.0002$, as determined by unpaired, two-tailed Student's *t* test against the empty vector control). (E) Model of BspA disruption of the MARCH6 E3 ligase complex. BspA interacts with MARCH6 at the ER membrane and interferes with the recruitment of UBXD8, which impairs the retrotranslocation of ERAD substrates and inhibits ERAD. Created using BioRender (www.biorender.com).

March6 and its proposed p97/VCP recruitment factor Ubxd8 (Fig. 4D to G). Based on their structural homology with their yeast orthologs Doa10 and Ubx2 (16–18, 35), mammalian MARCH6 and UBXD8 may interact and be functionally connected. We therefore hypothesized that BspA inhibits MARCH6-mediated ERAD by interfering with the interaction between MARCH6 and UBXD8. Immunoprecipitation of myc-tagged MARCH6 from HeLa cells producing myc-MARCH6, HA-tagged UBXD8, and 3×FLAG-BspA or not (Fig. 7A) showed coimmunoprecipitation of HA-UBXD8, demonstrating that mammalian MARCH6 and UBXD8 are part of the same ERAD complex. Interestingly, the presence of 3×FLAG-BspA strongly reduced the amount of UBXD8-HA

that coimmunoprecipitated with MARCH6 compared to control levels ($P < 0.0001$) (Fig. 7B), indicating that BspA interferes with MARCH6-UBXD8 interaction. To evaluate whether the effect of BspA on MARCH6-UBXD8 interaction functionally impairs MARCH6-dependent ERAD, we examined the steady-state levels of myc-MARCH6 itself as MARCH6 mediates its own degradation through ERAD via self-ubiquitination (10). 3×FLAG-BspA expression in HeLa cells producing myc-MARCH6 caused a striking increase in myc-MARCH6 steady-state level ($P = 0.0252$) (Fig. 7C), further arguing that BspA impairs MARCH6-dependent ERAD. Depletion of UBXD8 (71.9% ± 9.3%) in HeLa cells via siRNA (siUBXD8) treatment also caused a significant increase in myc-MARCH6 levels compared to nontargeting (siNT) control ($P = 0.0002$) (Fig. 7D), demonstrating that MARCH6-dependent ERAD is UBXD8-dependent in HeLa cells and its depletion phenocopies the effect of BspA. Taken together, these results demonstrate that BspA inhibits MARCH6-mediated ERAD by interfering with MARCH6-UBXD8 interaction (Fig. 7E).

DISCUSSION

A large number of intracellular microbial pathogens rely on host ER functions to undergo their infectious cycle, owing to the essential biosynthetic and homeostatic roles of this compartment. Among these microorganisms, *Brucella* heavily exploits the ER to generate its replicative niche and undergo intracellular proliferation (4, 24, 25, 27, 33, 34, 36), but how the bacterium modulates ER homeostatic functions for these purposes remains mostly unknown. Additionally, a role for the VirB T4SS in biogenesis of the ER-derived rBCV and intracellular growth has been long established (4, 5, 24, 25, 27, 34, 37, 38), yet how the dedicated T4SS effectors contribute to these processes is unclear, largely due to the limited knowledge about their identity and functions. Luizet et al. (8) recently showed that the *B. abortus* T4SS effector BspL enhances ERAD late in the *B. abortus* intracellular cycle (>48 hpi) to regulate the timing of aBCV formation and bacterial egress, establishing that *B. abortus* modulates ER protein quality control during its infectious cycle. Here, we demonstrate that the VirB T4SS effector BspA contributes to *B. abortus* intracellular growth by inhibiting the host ERAD pathway through targeting of the E3 ubiquitin ligase MARCH6-containing ERAD complex. This argues that *Brucella* uses T4SS effectors to modulate ER homeostatic functions, such as ERAD, for multiple purposes, as BspA exerts its function at least during the rBCV stage (24 hpi): i.e., at a temporally and functionally distinct step of the bacterium's intracellular cycle from BspL's intervention (8). These findings expand our understanding of bacterial effector-mediated modulation of ERAD, since BspA is to our knowledge the third effector to target mammalian ERAD, in addition to the T1SS substrate Ank4 of the obligate intracellular pathogen *O. tsutsugamushi* (22) and *B. abortus* BspL (8). Furthermore, consistent with our findings that the T4SS effector BspF promotes intracellular growth within rBCVs (25), BspA represents yet another *B. abortus* effector that plays a specific role in promoting bacterial growth within the ER-derived rBCV, confirming that type IV secretion by *B. abortus* is also dedicated to intracellular growth of the bacterium.

The mechanism by which BspA inhibits ERAD via disruption of the MARCH6-Ubxd8 interaction remains to be established. From a functional standpoint, BspA contains a single domain of unknown function, DUF2062, found in various prokaryotic proteins (23), which does not provide cues to its molecular mode of action on MARCH6. Topology predictions of BspA using the TMHMM-2.0 server (https://services.healthtech.dtu.dk/services/TMHMM-2.0/) suggested that BspA contains 4 transmembrane helices, consistent with its localization to ER membranes and interaction with MARCH6, but structure-function studies of BspA are needed to understand the structural basis of its interference with MARCH6 function. An additional challenge is the very limited number of known ERAD-targeting effectors in mammalian pathogens. Ank4 of *O. tsutsugamushi* exerts its mode of action through interaction with the ERAD component Bat3 (22), and *B. abortus* BspL targets another ERAD components, Herp, in order to enhance ERAD activity (8). Several plant pathogens target the host proteostatic machinery via effectors that have been recently classified (19) based on the concept of effector-targeted

pathways (ETPs) (39) and their mode of action on the host proteolytic mechanisms. BspA classifies as a "stabilizer," a group of viral and bacterial effectors that use various mechanisms to prevent degradation of target host proteins, including masking of substrate degron motifs (40), up- or downmodulation of the E3 ligase activity (41–43), substrate deubiquitination (44, 45), or disturbance of E3 ligase complexes (46, 47). Our finding that BspA interferes with MARCH6-UBXD8 interaction places it in the latter category, as a first bacterial effector together with the viral effectors p25 and β-C1 (46, 47). Whether BspA exerts an additional effect on MARCH6 activity itself remains to be determined.

The pathogenic strategy behind BspA's targeting of the MARCH6-UBXD8 branch of the ERAD pathway is currently unknown and requires further investigation. The MARCH6 E3 complex in mammals is very poorly understood, both structurally and functionally. Most of our knowledge of MARCH6 function in ERAD comes from research on its yeast homologue, Doa10. Doa10 functions together with two separate E2 ubiquitin-conjugating enzymes, Ubc6 and Ubc7, to facilitate substrate ubiquitination (35, 48). Substrate extraction from the ER membrane is energetically facilitated by the ATPase Cdc48/p97, together with its two protein cofactors Ufd1 and Npl4 (49, 50). This step is conserved among all ERAD branches and the recruitment of this complex to the various E3 complexes is facilitated by Cdc48 interacting motif-containing protein cofactors, including UBX domain-containing adaptors (17, 18, 51). Cdc48/p97 is a multifunctional protein whose roles extend beyond the ERAD pathway, and its functional specificity is determined by two categories of cofactors (51, 52): (i) major cofactors such as the heterodimer Ufd1-Npl4 or the Shp1, eyes-closed, p47 (SEP)-domain adapter p37, which typify distinct modes of client targeting, and (ii) additional substrate-recruiting cofactors such as Ubx2 (UBXD8 in mammals) that determine ERAD substrate specificity, including for the Doa10/MARCH6 E3 complex (17, 18). Hence, a tempting hypothesis is that *B. abortus* specifically targets MARCH6-dependent ERAD to prevent degradation of host proteins or ER-associated *B. abortus* effectors that are targeted by this branch and are required for optimal intracellular replication. In support of this hypothesis, (i) ERAD inhibition with kifunensine restored the replication of the Δ*bspA* deletion mutant but did not increase that of wild-type bacteria, suggesting that general ERAD deficiency does not overly benefit *B. abortus* intracellular growth, (ii) siRNA-mediated depletion of March6 and Ubxd8, but not Hrd1, phenocopied the effect of kifunensine, arguing that BspA-mediated effect on ERAD occurs predominantly via the March6-Ubxd8 branch, and (iii) we previously showed that ectopically expressed BspA does not induce ER stress (23), a likely consequence of general ERAD inhibition, as caused by the *O. tsutsugamushi* effector Ank4 (22). However, Ubxd8 depletion in macrophages also affected *B. abortus* replication under conditions that did not affect ERAD activity, arguing that Ubxd8 may also contribute to bacterial replication via an ERAD-independent function.

How inhibition of MARCH6-dependent ERAD promotes *B. abortus* intracellular growth remains to be determined. While the possibility that BspA inhibits MARCH6-dependent ERAD to counteract degradation of ER-associated *Brucella* effectors needs to be examined, an alternative hypothesis stems from the functional link between MARCH6, ERAD, and host sterol homeostasis, an important host function for intracellular bacteria (53, 54). MARCH6 regulates the sterol-dependent degradation of the enzyme squalene monooxygenase (SQLE), which is part of the mevalonate pathway (13, 55, 56), and cholesterol increases the intracellular levels of MARCH6 and stimulates MARCH6-dependent ERAD (57). MARCH6 has also emerged as a regulator of lipid droplet content through degradation of the structural protein perilipin 2 (14). Our findings have uncovered a functional connection between MARCH6 and UBXD8 in mammals, as we have shown that UBXD8 is part of the MARCH6 E3 complex and is involved in MARCH6 stability. Besides its involvement in ERAD, UBXD8 also regulates cholesterol biosynthesis and homeostasis of lipid droplets, a complex cellular depot for neutral lipids and sterols (58, 59), an additional function that may explain its ERAD-independent contribution to *B. abortus* replication. Hence, *B. abortus* may target the MARCH6-UBXD8 branch of ERAD to modulate host sterol biosynthesis or lipid storage, both of which are host processes important to bacterial intracellular pathogenesis (54, 60). While the role of cholesterol in *Brucella* infection has been studied in the context of

bacterial entry (61, 62), whether lipid droplet metabolism contributes to *Brucella* intracellular replication has not been studied. Hence, our findings on the role of BspA in *B. abortus* intracellular replication uncover further involvement of the host ERAD pathway in *Brucella* pathogenesis that may extend beyond regulation of ER proteostasis.

MATERIALS AND METHODS

Bacterial strains and culture. *Brucella abortus* strains 2308, 2308 Δ*virB11*, and 2308 Δ*bspA* have been described previously (23, 63). Routinely, all strains were first grown for 3 days at 37°C in a 5% CO_2 atmosphere on tryptic soy agar (TSA) (Difco; 236950) and then in tryptic soy broth (TSB) (Difco; 211825) at 37°C until an optical density at 600 nm (OD_{600}) of 0.8 was reached. *B. abortus* 2308 Δ*bspA*::*bspA* strain was constructed by genetic complementation of the Δ*bspA* mutant with a single copy of *bspA* via chromosomal insertion. For this purpose, a 576-bp DNA fragment containing *bspA* (BAB1_0678) and a 250-bp fragment upstream of BAB1_0677containing the *bspA* native promoter were PCR amplified using primers WSU0212 and WSU0215 and WSU213 and WSU214, respectively. The two fragments were then fused by overlapping extension PCR and cloned into pUC18T-miniTn7K-dsRed using EcoRI and KpnI restriction sites. The resulting pUC18T-miniTn7K-dsRed-*bspA* construct was verified by sequencing and subsequently electroporated into *B. abortus* 2308 Δ*bspA* as previously described (25). All experiments involving *B. abortus* were performed in a biosafety level 3 facility in accordance with standard operating procedures approved by the Washington State University Institutional Biosafety Committee and in compliance with the CDC/USDA Federal Select Agents Program. The *Escherichia coli* strains (DH5α) (Invitrogen) used for molecular cloning were grown either on Luria-Bertani agar or broth (Difco LB Lennox; BD [240110 and 240230, respectively]), supplemented with 100 μg/mL of ampicillin or 50 μg/mL of kanamycin when needed.

Mammalian cell culture. Murine bone marrow-derived macrophages (BMMs) were obtained as described previously (25). Briefly, bone marrow cells of 6- to 12-week-old C57BL/6J mice (Jackson Laboratory; 000664) were harvested and differentiated into macrophages for 5 days at 37°C in a 10% CO_2 atmosphere in Dulbecco's modified Eagle's medium (DMEM) (containing 1 g/L glucose, L-glutamine, and sodium pyruvate) (Corning; 10014), supplemented with 10% fetal bovine serum (FBS) (Atlanta Biologicals S10350H) and 20% L-929 mouse fibroblast-conditioned medium (L-CSF), in non-tissue culture-treated dishes (Falcon; 351058). After 5 days of incubation, nonadherent cells were washed out using cold phosphate-buffered saline (PBS) (Corning; 21-040-CV) and macrophages were harvested in prechilled, cation-free PBS (Corning; 21-030-CV), supplemented with 1 g/L D-glucose, and seeded into 6- or 24-well tissue culture-treated plates at a density of 1×10^6 or 5×10^4 cells/well, respectively. When microscopy analysis was required, BMMs were seeded into 24-well plates onto 12-mm-diameter glass coverslips at a density of 5×10^4 cells/well. HeLa cells (ATCC clone CCL-2) were routinely grown at 37°C in a 5% CO_2 atmosphere in minimum essential medium (MEM) (Corning; 15010) supplemented with 2 mM L-glutamine and 10% FBS. HEK293T cells (ATCC CRL-11268) were cultured in Dulbecco's modified Eagle's medium (DMEM) containing 4.5 g/L glucose and sodium pyruvate (Corning; 15013).

Construction of mammalian and retroviral expression vectors. All PCR primers used in this work are described in Table 1. pCMV-3×FLAG-BspA was generated by amplification of *bspA* from genomic DNA of *B. abortus* 2308 using primers WSU0160 and WSU0161 and cloned into p3×FLAG-CMV-7.1 using EcoRI and KpnI restriction sites. Human *MARCH6* cDNA was obtained from OriGene (pCMV6-AC-GFP-MARCH6) (OriGene; RG222261). myc-MARCH6 was constructed by amplification of the *MARCH6* gene using primers WSU0022 and WSU0002, followed by cloning into pCMV-myc (Clontech; 635690) using EcoRI and BamHI restriction sites. Construction of pcDNA3.1-NHK-HA has been previously described (32). pCLXSN-NHK-HA was obtained by amplification of *NHK-HA* from pcDNA3.1-NHK-HA using primers WSU0638 and WSU0665, followed by cloning into pCLXSN-MCS2 (24) using EcoRI and SalI restriction sites. Type 2 iodothyronine deiodinase (D2)-encoding cDNA was kindly provided by Balazs Gereben, Hungarian Academy of Sciences (12). C-terminally 3×FLAG-tagged D2 was constructed by amplification of the *D2* gene using primers WSU0607 and WSU0768 and cloning into pcDNA3.1(−) using EcoRI and BamHI restriction sites. The D2-3×FLAG construct was confirmed by sequencing and excised from pcDNA3.1-D2-3×FLAG using the same restriction sites and subsequently transferred into pCLXSN-MCS2. The construction of pcDNA3.1-A1AT-NHK-ddVenus has been described elsewhere (25) and was kindly provided by P. Cresswell, Yale University School of Medicine. Human *UBXD8* cDNA was procured from Addgene (no. 53777), and construct pcDNA3.1-UbxD8-HA was obtained by amplification of the *UBXD8* gene from pRK-FLAG-UbxD8 (64) using primers WSU0636 and WSU0637, followed by cloning into pcDNA3.1(−) using the EcoRI and BamHI restriction sites. All constructs were confirmed by DNA sequencing.

siRNA silencing in macrophages. About 1×10^6 freshly differentiated BMMs were electroporated with 2 to 3 nmol of either nontargeting siRNA ON-TARGETplus SMARTpool (GE Dharmacon; D-001810-10-20) or siRNAs specific for either mouse *March6* (L-055065-01-0005), mouse *Hrd1* (L-041789-01-0005), or mouse Ubxd8 (L-059272-01-0005) using the mouse macrophage Nucleofector kit (Lonza; VPA-1009) in an Amaxa Nucleofector II apparatus (Lonza). BMMs were immediately recovered after pulsing in macrophage complete medium, plated onto either 24-well plates (for infections) or 6-well plates (for quantification of depletion), and incubated for 72 h prior to infection at 37°C in a 10% CO_2 atmosphere. Target depletion was monitored and quantified by Western blotting (Hrd1 and Ubxd8) or quantitative reverse transcription-PCR (RT-qPCR) (*March6*).

Quantification of *MARCH6* knockdown efficiency by RT-qPCR. Total RNA of BMMs treated with either nontargeting or *March6*-specific siRNAs was extracted as follows. At 72 h postnucleofection, cells

TABLE 1 List of primers used in this study

Primer	Sequence (5′→3′)	Use
WSU0212	AGCTCGAATTCTTGCTACTCCGAAGATGAAATCC	Amplification of *bspA* gene for construction of pUC18T-miniTn7K-dsRed-*bspA*
WSU0215	GGATATCTGCGTTGGAACAACATCAAGCTCTCCGGCGGCGGCAAA	
WSU0213	AAGGTACCTCATGCCTTCTGCAACTCC	Amplification of *bspA* native promoter region for construction of pUC18T-miniTn7K-dsRed-*bspA*
WSU0214	ATGTTGTTCCAACGCAGATATC	
WSU0002	CGCGGATCCTTACAGGTCCTCCTCTGAGATCAGCTTCTGCTCTTCTT GGGATGACTGTGGAGGTGG	Cloning of *MARCH6* in pCMV-myc
WSU0022	CCGGAATTCGCCACCATGGACACCGCGGAGGAAGAC	
WSU0638	CGCGAATTCGCCACCATGCCGTCTTCTGTCTCGTGG	Cloning of NHK-HA in pCLXSN-MCS2
WSU0665	GATCTCGGTCGACTTAAGCGTAATCTGGAACATCGTATGGGTATGC ACGGCCTTGGAGAGC	
WSU0607	GGCCCGAATTCGCCACCATGGGCATCCTCAGCGTAGACTTGC	Cloning of D2-3×FLAG in pcDNA3.1(−)
WSU0768	CGCGGATCCCTACTTGTCATCGTCATCCTTGTAATCGATGTCATGAT CTTTATAATCACCGTCATGGTCTTTGTAGTCACCAGCTAATCTAG TTTTCTTACATCTC	
WSU0636	GGCCCGAATTCGCCACCATGGCGGCGCCTGAGG	Cloning of *UBXD8* in pcDNA3.1(−)
WSU0637	CGCGGATCCTCAAGCGTAATCTGGAACATCGTATGGGTATTCGTCA GTTAGGTCCTGAAC	
WSU0268	CTCAGTGGTGGTTGAAAACTGT	Quantification of *March6* mRNA by RT-qPCR
WSU0269	GCGCCAGAAGCTATGACATAC	
WSU0201	TGAGATTCGGGATATGCTGTTGG	Quantification of *rplp0* mRNA by RT-qPCR
WSU0202	CGGGTCCTAGACCAGTGTTCT	
RC255	CATGGAGGCCGAATTCTTGTTCCAACGCAGATAT	Cloning of *bspA* in pGBKT7
RC256	GCAGGTCGACGGATCCTGCCTTCTGCAACTCCCGCTG	
RC437	GGAGGCCAGTGAATTCGACACCGCGGAGGAAGACATA	Cloning of *MARCH6* in pGBKT7
RC438	CGAGCTCGATGGATCCTCTTGGGATGACTGTG	

were washed 3 times in 1× PBS and lysed in 1 mL of ice-cold TRIzol reagent (Invitrogen; 15596018) by gentle pipetting. After incubation for 5 min at room temperature, 200 μL of chloroform (Sigma; C2432) was added to each sample, followed by brief mixing, incubation for 10 min at room temperature, and centrifugation for 10 min at 16,000 × *g* at 4°C. The aqueous supernatants were transferred into new tubes, and total RNA was precipitated by the addition of 10 mg of glycogen (Invitrogen; AM9510) and 500 μL of isopropanol (Sigma; I9516), followed by incubation for 10 min at room temperature and centrifugation for 30 min at 16,000 × *g* at 4°C. Supernatants were discarded, and the RNA pellets were washed in ice-cold 75% ethanol, followed by centrifugation for 15 min at 16,000 × *g* at 4°C and drying for 10 min at room temperature. RNA pellets were resuspended in nuclease-free water, and residual DNA was removed using the Turbo DNA-free kit (Invitrogen; AM1907) according to the manufacturer's recommendation. Finally, cDNA was synthesized using the Maxima H Minus first-strand cDNA synthesis kit (Thermo; K1681) following the provider's protocol. RT-qPCR was performed using the Luminaris color HiGreen qPCR master mix (Thermo; K0393) according to the manufacturer's recommendations in a Bio-Rad CFX96 thermal cycler under default baseline and threshold settings. Relative *march6* mRNA was determined using primers WSU0268 and WSU0269. Results were normalized against *rplp0* expression, determined with primers WSU0201 and WSU0202.

Retroviral transduction. Retroviral supernatants were prepared by seeding HEK293T cells into 10-cm tissue culture dishes (Thermo; 172931) at a density of 2.5×10^6 cells/plate. At 24 h postseeding, the cells were cotransfected with the ecotropic helper plasmid pCL-Eco (Imgenex, Novus Biologicals; NBP2-29540) and pCLXSN derivatives using the FuGENE 6 transfection reagent (Promega; E2692) according to the manufacturer's recommendation. At 48 h posttransfection, the retroviral supernatants were collected, filtered through 0.45-μm-pore filter, and aliquoted. BMMs were transduced by adding retroviral supernatant to the growth medium in a 2:5 ratio, followed by 48 h of incubation.

Antibodies. The following antibodies were used for immunofluorescence: rat monoclonal anti-LAMP1 (1:400, clone 1D4B) (obtained from the Developmental Studies Hybridoma Bank and developed under the auspices of the NICHD and maintained by the University of Iowa, Department of Biological sciences, Iowa City, IA), mouse monoclonal anti-FLAG (1:500, clone M2) (Sigma; F1804), monoclonal rabbit anti-myc (1:500, clone 71D10) (Cell Signaling; 2278), monoclonal rat anti-BAP31 (1:500, clone CC-1) (Invitrogen; MA3-002), Alexa Fluor 488-conjugated anti-rat IgG or antimouse IgG, and Alexa Fluor 568-conjugated anti-rabbit IgG and Cy5-conjugated anti-rat donkey antibodies (1:500) (Invitrogen, Life Technologies). The following primary antibodies were used for Western blotting: polyclonal rabbit anti-FLAG (1:5,000) (Invitrogen; 740001), monoclonal mouse anti-FLAG (1:10,000, clone M2) (Millipore Sigma; F1804), mouse monoclonal anti-myc (1:5,000, clone 9E10) (Invitrogen; MA1-980), rabbit monoclonal anti-HA (1:5,000, clone C29F4) (Cell Signaling; 3724), mouse monoclonal anti-β-actin (1:20,000, clone 8H10D10) (Cell Signaling; 3700), rabbit polyclonal anti-Hrd1 (1:10,000) (Proteintech; 13473-1-AP), rabbit monoclonal anti-UBXD8 (1:5,000, clone D8H6D) (Cell Signaling; 34945). Goat anti-mouse light-chain IgG

conjugated with horseradish peroxidase (HRP) (1:10,000) (AffiniPure) (Jackson Laboratories; 115-005-174), horse anti-mouse heavy-plus-light-chain IgG-HRP (1:10,000) (Cell Signaling; 7076), goat anti-rabbit heavy-plus-light-chain IgG-HRP (1:10,000) (Cell Signaling; 7074), and goat anti-rabbit IgG Fc-HRP (1:10,000) (Invitrogen; A16116) were used as secondary antibodies.

Immunofluorescence microscopy. Mammalian cells grown on 12-mm glass coverslips were washed three times in 1× PBS and then fixed for 20 min in 3% paraformaldehyde (PFA) (EMD; 818715) in 1× PBS, followed by quenching for 30 min at room temperature in 1× PBS containing 50 mM ammonium chloride. Samples were then blocked and permeabilized for 30 min in 1× PBS containing 0.1% (wt/vol) saponin and 10% (vol/vol) horse serum, followed by immunostaining for 45 min at room temperature in a humidified chamber. The coverslips were then briefly washed, first in 1× PBS containing 0.1% saponin and then in 1× PBS only, followed by immunostaining for 45 min at room temperature in a humidified chamber with fluorophore-conjugated secondary antibodies. Finally, the samples were washed first in 1× PBS, and then in distilled H_2O, and mounted in Mowiol mounting medium (EMD; 475904) on microscopy slides. Microscopic observation was performed with either a Leica DM4000 epifluorescence upright microscope or Leica SP8 confocal laser-scanning microscope.

Western blotting. Bacterial or mammalian cells were lysed in 2× SDS-PAGE sample buffer (0.12 M Tris [pH 6.8], 10% [vol/vol] glycerol, 3.4% [wt/vol] SDS, 0.2 M dithiothreitol [DTT], 0.004% [wt/vol] bromophenol blue). All samples were denatured for 10 min at 95°C, except for those containing overexpressed myc-MARCH6, which were denatured for 10 min at 60°C due to protein aggregation at higher temperatures. All samples were loaded in equal volumes and resolved by SDS-PAGE, followed by transfer onto 0.22-μm-pore nitrocellulose membranes (Cytiva; 10600004). Membranes were subsequently blocked for 1 h at room temperature with rocking in TBST buffer (0.14 M NaCl, 0.02 M Tris [pH 7.6], 0.1% [wt/vol] Tween 20) supplemented with 5% (wt/vol) nonfat dry skim milk. Primary immunostaining was performed overnight at 4°C with rocking, followed by probing with HRP-conjugated secondary antibodies for 1 h at room temperature with rocking, in blocking buffer. Immunoblots were then developed with the Super Signal West Femto maximum-sensitivity substrate (Thermo; 34096) and imaged using a Bio-Rad ChemiDoc imaging system. Representative figures were assembled using Adobe Photoshop 2023 suite.

Macrophage infection assay. For macrophage infection with *Brucella abortus*, bacterial suspensions were prepared in prechilled macrophage complete medium from early-logarithmic-phase bacterial cultures and added to BMMs at multiplicity of infection (MOI) of 10. Bacterial entry was synchronized by centrifugation for 10 min at 400 × *g* at 4°C, followed by incubation for 20 min at 37°C in a 10% CO_2 atmosphere. Extracellular bacteria were then removed by 5 washes in prewarmed DMEM and treatment with 100 μg/mL gentamicin (Gibco; 15710-072) in complete macrophage medium between 1 and 2 hpi. Finally, the gentamicin was washed out and macrophages were incubated in complete macrophage medium for the remainder of the experiment.

rBCV biogenesis and bacterial replication assays. BMMs were seeded onto 12-mm glass coverslips in 24-well plates and infected with a panel of $DsRed_m$-expressing *B. abortus* strains in a time course experiment over a 24-h period, during which coverslips were collected at 4, 8, 12, and 24 hpi, washed 3 times in 1× PBS, fixed for 20 min in 3% PFA, and immunostained for the LAMP1 endosomal marker. The processed samples were then mounted blind on glass slides, and at least 100 individual BCVs were analyzed at each time point by epifluorescence microscopy for LAMP1-positive staining. Bacterial replication was quantified by scoring the numbers of intracellular bacteria at 24 hpi in at least 100 infected individual BMMs in a series of random microscopy fields. Both assays were repeated independently at least 3 times.

Immunoprecipitation. Reciprocal coimmunoprecipitation of ectopically expressed 3×FLAG-tagged BspA and myc-tagged MARCH6 were performed in HeLa cells. HeLa cells were seeded into 10-cm tissue culture dishes at a density of 1 × 10^6 cells/plate and transfected using FuGENE 6 transfection reagent according to the manufacturer's recommendation. For coimmunoprecipitation of myc-MARCH6 with 3×FLAG-BspA, cells were cotransfected (1:1 plasmid ratio) with pCMV-myc-MARCH6 and either empty pCMV-3×FLAG or pCMV-3×FLAG-bspA, while cells were cotransfected with pCMV-3×FLAG-bspA and either empty pCMV-myc or pCMV-myc-MARCH6 for coimmunoprecipitation of 3×FLAG-BspA with myc-MARCH6. For coimmunoprecipitation of UBXD8-HA with myc-MARCH6 in the presence or absence of 3×FLAG-BspA, HeLa cells were cotransfected (1:1:1 plasmid ratio) with either empty pCMV-myc, pcDNA3.1-UBXD8-HA, and empty pCMV-3×FLAG, empty pCMV-myc, pcDNA3.1-UBXD8-HA, and pCMV-3×FLAG-BspA, pCMV-myc-MARCH6, pcDNA3.1-UBXD8-HA, and empty pCMV-3×FLAG, or pCMV-myc-MARCH6, pcDNA3.1-UBXD8-HA, and pCMV-3×FLAG-BspA. After 24 h of transfection, cells were washed 3 times in prechilled 1× PBS and either directly lysed in 0.5 mL of lysis buffer (50 mM Tris [pH 7.5], 300 mM NaCl, 0.5% [vol/vol] Triton X-100) (EMD; 648466) and (1:500 HALT protease inhibitor cocktail [Thermo Fisher; 78429]) or, when myc-MARCH6 was immunoprecipitated, first subjected to cross-linking for 2 h with 0.5 mM dithiobis(succinimidylpropionate) (DSP) (Thermo; 22586) and then lysed in 0.5 mL of lysis buffer. Lysates were then collected and incubated for 30 min at 4°C with gentle rotation, clarified for 5 min at 12,000 × *g* at 4°C, and precleared with lysis buffer-conditioned protein A-conjugated paramagnetic beads (Thermo; 88846) for 1 h at 4°C with gentle rotation. The precleared lysates were then incubated with either anti-FLAG- or anti-myc-conjugated paramagnetic beads (Sigma, M8823, and Thermo, 88843, respectively) for 2 h at 4°C with gentle rotation, followed by 10 washes in lysis buffer and elution of the bound proteins for 5 min at 60°C in 50 μL of elution buffer (120 mM Tris [pH 6.8], 1% [vol/vol] glycerol, 120 mM SDS and 0.4% bromophenol blue). Eluates and input lysates were resolved by SDS-PAGE and Western blotting, and quantification of band intensities was performed by densitometry using ImageLab 6.1 (Bio-Rad).

Yeast two-hybrid screen. The Matchmaker Gold yeast two-hybrid system (TaKaRa; 630489) was used to screen a human bone marrow cDNA library against a Gal4 binding domain (BD) fusion of BspA as previously described (25). Briefly, *bspA* was amplified without its START and STOP codons from genomic DNA of *B. abortus* 2308 using primers RC255 and RC256 and cloned between the EcoRI and BamHI restriction sites of pGBKT7 using the In-Fusion PCR cloning system (Clontech; 639650). The obtained pGBKT7-*bspA* construct was verified by sequencing and then transformed into the Y2HGold yeast strain using the Yeastmaker yeast transformation system 2 kit (Clontech; 630439). Screening was performed according to the Matchmaker Gold yeast two-hybrid system's protocol by mating the pGBKT7-*bspA*-containing Y2HGold strain against *S. cerevisiae* host strain Y187, transformed with a Mate & Plate human bone marrow cDNA library (TaKaRa; 630477), which was cloned into the yeast GAL4 activation domain (AD)-containing vector pGADT7-Rec. Mating of the yeast Y187 strain, containing a pGADT7 fusion of simian virus 40 large T antigen (pGADT7-T) with the Y2HGold strain, containing a pGBKT7 fusion of murine p53 protein (pGBKT-p53), served as positive control. Matings of the Y187 strain containing empty pGADT7 with Y2HGold strains, containing either empty pGBKT7 or pGBKT7-*bspA*, were used as negative controls. Production of GAL4-BD and GAL4-AD fusions was confirmed by Western blotting. The full-length MARCH6 construct pGADT7-MARCH6$_{full}$ was generated by amplifying the *MARCH6* gene from pCMV6-AC-GFP-MARCH6 using primers RC437 and RC438 and then cloning it into pGADT7 using EcoRI and BamHI restriction sites.

Pharmacological inhibition of ERAD during *B. abortus* infection. Freshly differentiated BMMs were seeded onto 12-mm glass coverslips in either 24-well plates (for intracellular replication assays) or 6-well plates (for Western blot analysis). At 24 h postseeding, the treatment control plates were transduced to express NHK-HA using retroviral supernatants and incubated for 48 h at 37°C in 10% CO_2. BMMs seeded on coverslips were infected at an MOI of 10 with either the wild-type *B. abortus* 2308, Δ*bspA* mutant, or Δ*bspA*::*bspA* strain for 24 h. BMMs were treated at 2 hpi (to avoid interference with bacterial uptake) with 1.5 μM kifunensine (Cayman Chemicals; 10009437) for a total of 22 h. At 24 hpi, infected coverslips were processed for fluorescence microscopy analysis of bacterial replication, while NHK-HA-producing BMMs were washed 3 times in 1× PBS, lysed in 2× SDS-PAGE sample buffer, and resolved by SDS-PAGE for Western blot analysis. The relative steady-state levels of NHK-HA served as a readout for ERAD inhibition and were determined by quantitative Western blotting using β-actin as loading control.

ERAD substrate stability assays in BMMs. To measure NHK-HA stability in BMMs during *B. abortus* infection, freshly differentiated BMMs were seeded into 6-well cell culture-treated plates at density of 3×10^5 cells/well and incubated at 37°C in a 10% CO_2 atmosphere for 72 h prior to infection. At 24 h postseeding, the cells were transduced with pCLXSN-NHK-HA for 48 h and then either mock infected or infected with the wild-type 2308 or Δ*bspA* mutant *B. abortus* strain for 24 h at an MOI of 1,000. At 24 hpi, cells were washed three times in sterile 1× PBS, lysed in 100 μL of 2× SDS PAGE sample buffer, and then inactivated for 10 min at 100°C. Samples were then resolved by SDS-PAGE and probed for NHK-HA by Western blotting. Steady-state-levels of NHK-HA were quantified by densitometry and normalized to β-actin as the loading control. To measure NHK-HA and D2-3×FLAG stability in BMMs expressing or not expressing 3×FLAG-BspA, freshly differentiated BMMs were seeded into 6-well tissue culture-treated plates at a density of 3×10^5 cells/well, incubated at 37°C in 10% CO_2 for 24 h, and then cotransduced with retroviral supernatants of either pCLXSN-NHK-HA and empty pCLXSN, pCLXSN-NHK-HA and pCLXSN-3×FLAG-BspA, pCLSXN-D2-3×FLAG and empty pCLXSN, or pCLXSN-D2-3×FLAG with pCLXSN-3×FLAG-BspA. After 72 h of transduction, cells were washed three times in sterile 1× PBS, lysed in 100 μL of 2× SDS-PAGE sample buffer, and then boiled for 10 min at 100°C. Samples were then resolved by SDS-PAGE and probed for either NHK-HA or D2-3×FLAG and 3×FLAG-BspA by Western blotting. Steady-state levels of either NHK-HA or D2-3×FLAG were quantified by densitometry and normalized to β-actin as the loading control.

NHK-ddVenus fluorescence ERAD assay. To measure NHK-ddVenus fluorescence in BspA-expressing cells, HeLa cells seeded into a 24-well plate on glass coverslips (3.5×10^4/well) were cotransfected for 21 h with pcDNA3.1-NHK-ddVenus and either pmCherry or pCMV-3×FLAG-BspA, according to the FuGENE 6 manufacturer's instructions. To measure NHK-ddVenus fluorescence in *B. abortus*-infected cells, HeLa cells seeded into a 24-well plate on glass coverslips (3.5×10^4/well) were first mock infected or infected with DsRed$_m$-expressing bacteria as described above. At 2 h postinfection, cells were transfected with pcDNA3.1-NHK-ddVenus following the FuGENE 6 manufacturer's instructions. At 21 h posttransfection or postinfection, the medium was replaced with complete medium containing (S)-MG132 (10 μg/mL) (Cayman Chemicals; 10012628) for 3 h. Cells were then fixed in 3% PFA in 1× PBS for 20 min at 37°C, and nuclei were counterstained with Hoechst's stain (Invitrogen; H3570). Coverslips were mounted blind onto glass slides for analysis via confocal microscopy. NHK-ddVenus-producing HeLa cells that expressed either mCherry or 3×FLAG-BspA or that were either infected or not infected (mock infected) were imaged and analyzed for NHK-ddVenus fluorescence intensity using Fiji ImageJ (Fiji 2.1.0). Individual cells were selected by the Freehand ROI tool, and area, integrated density, and mean gray value were recorded. Mean fluorescence intensity for each cell was quantified by multiplying the cell area by the mean fluorescence of background readings subtracted from the integrated density. Eighty to 100 cells per condition were analyzed from three independent experiments.

MARCH6 stability assays in HeLa cells. To measure MARCH6 stability in the presence or absence of BspA, HeLa cells were seeded into 6-well cell culture-treated plates at a density of 1.4×10^5 cells and cotransfected 24 h after being seeded with pCMV-myc-MARCH6 and either pCMV-3×FLAG or pCMV-3×FLAG-BspA using FuGENE 6 reagent (Promega). At 24 h posttransfection, samples were washed three times in 1× PBS, lysed in 2× SDS-PAGE sample buffer, and resolved by SDS-PAGE. myc-MARCH6 and

3×FLAG-BspA were detected using Western blotting, and MARCH6 levels were quantified by densitometry analysis and normalized to β-actin as the loading control. UBXD8 depletion was performed in HeLa cells seeded into 6-well cell tissue culture-treated plates (1.4×10^5 cell/well) via transfection with either with 50 pmol of nontargeting siRNA ON-TARGETplus SMARTpool (GE Dharmacon; D-001810-10-20) or siRNA against human UBXD8 (L-010649-02-0005) using DharmaFECT 1 transfection reagent (GE Dharmacon) according to the manufacturer's recommendation. After 48 h, the growth medium was replenished, and cells were transfected with pCMV-myc-MARCH6 using FuGENE 6 reagent (Promega) and collected 24 h posttransfection for Western blot analysis of UBXD8 depletion and MARCH6 steady-state levels.

Data quantification and statistical analysis. All results are presented as the means ± standard deviations (SD) of data from at least three independent experiments. Statistical significance was determined using either an unpaired, two-tailed Student's *t* test or one- or two-way analysis of variance (ANOVA), followed by Dunnett's multiple-comparison test. A *P* value of <0.05 was considered significant. The specific tests used for the various data sets are indicated in the corresponding figure legends.

ACKNOWLEDGMENTS

We thank Kelsey Binder, Jennifer Cundiff, and Kiara Held for technical assistance and Peter Cresswell and Balazs Gereben for the gift of plasmids.

This work was supported by funding from the National Institute of Allergy and Infectious Diseases, National Institutes of Health (AI127830 and AI129992) to Jean Celli, NIH T32 training grant GM008336 and a Poncin fellowship to Elizabeth Borghesan, and NIH T32 training grant AI007025 and a USDA NIFA postdoctoral fellowship 2016-67012-25179 to Cheryl N. Miller. The funders had no role in study design, data collection and interpretation, or the decision to submit the work for publication.

REFERENCES

1. Vaughn B, Abu Kwaik Y. 2021. Idiosyncratic biogenesis of intracellular pathogens-containing vacuoles. Front Cell Infect Microbiol 11:722433. https://doi.org/10.3389/fcimb.2021.722433.
2. Celli J. 2019. The intracellular life cycle of Brucella spp. Microbiol Spectr 7. https://doi.org/10.1128/microbiolspec.BAI-0006-2019.
3. Pappas G, Papadimitriou P, Akritidis N, Christou L, Tsianos EV. 2006. The new global map of human brucellosis. Lancet Infect Dis 6:91–99. https://doi.org/10.1016/S1473-3099(06)70382-6.
4. Celli J, de Chastellier C, Franchini D-M, Pizarro-Cerda J, Moreno E, Gorvel J-P. 2003. Brucella evades macrophage killing via VirB-dependent sustained interactions with the endoplasmic reticulum. J Exp Med 198:545–556. https://doi.org/10.1084/jem.20030088.
5. Comerci DJ, Martinez-Lorenzo MJ, Sieira R, Gorvel J-P, Ugalde RA. 2001. Essential role of the VirB machinery in the maturation of the Brucella abortus-containing vacuole. Cell Microbiol 3:159–168. https://doi.org/10.1046/j.1462-5822.2001.00102.x.
6. Starr T, Child R, Wehrly TD, Hansen B, Hwang S, López-Otin C, Virgin HW, Celli J. 2012. Selective subversion of autophagy complexes facilitates completion of the Brucella intracellular cycle. Cell Host Microbe 11:33–45. https://doi.org/10.1016/j.chom.2011.12.002.
7. Starr T, Ng TW, Wehrly TD, Knodler LA, Celli J. 2008. Brucella intracellular replication requires trafficking through the late endosomal/lysosomal compartment. Traffic 9:678–694. https://doi.org/10.1111/j.1600-0854.2008.00718.x.
8. Luizet J-B, Raymond J, Lacerda TLS, Barbieux E, Kambarev S, Bonici M, Lembo F, Willemart K, Borg J-P, Celli J, Gérard FCA, Muraille E, Gorvel J-P, Salcedo SP. 2021. The Brucella effector BspL targets the ER-associated degradation (ERAD) pathway and delays bacterial egress from infected cells. Proc Natl Acad Sci U S A 118:e2105324118. https://doi.org/10.1073/pnas.2105324118.
9. Christianson JC, Carvalho P. 2022. Order through destruction: how ER-associated protein degradation contributes to organelle homeostasis. EMBO J 41:e109845. https://doi.org/10.15252/embj.2021109845.
10. Hassink G, Kikkert M, van Voorden S, Lee S-J, Spaapen R, van Laar T, Coleman CS, Bartee E, Früh K, Chau V, Wiertz E. 2005. TEB4 is a C4HC3 RING finger-containing ubiquitin ligase of the endoplasmic reticulum. Biochem J 388:647–655. https://doi.org/10.1042/BJ20041241.
11. Schulz J, Avci D, Queisser MA, Gutschmidt A, Dreher L-S, Fenech EJ, Volkmar N, Hayashi Y, Hoppe T, Christianson JC. 2017. Conserved cytoplasmic domains promote Hrd1 ubiquitin ligase complex formation for ER-associated degradation (ERAD). J Cell Sci 130:3322–3335. https://doi.org/10.1242/jcs.206847.
12. Zavacki AM, Arrojo e Drigo R, Freitas BCG, Chung M, Harney JW, Egri P, Wittmann G, Fekete C, Gereben B, Bianco AC. 2009. The E3 ubiquitin ligase TEB4 mediates degradation of type 2 iodothyronine deiodinase. Mol Cell Biol 29:5339–5347. https://doi.org/10.1128/MCB.01498-08.
13. Zelcer N, Sharpe LJ, Loregger A, Kristiana I, Cook ECL, Phan L, Stevenson J, Brown AJ. 2014. The E3 ubiquitin ligase MARCH6 degrades squalene monooxygenase and affects 3-hydroxy-3-methyl-glutaryl coenzyme A reductase and the cholesterol synthesis pathway. Mol Cell Biol 34:1262–1270. https://doi.org/10.1128/MCB.01140-13.
14. Nguyen KT, Lee C-S, Mun S-H, Truong NT, Park SK, Hwang C-S. 2019. N-terminal acetylation and the N-end rule pathway control degradation of the lipid droplet protein PLIN2. J Biol Chem 294:379–388. https://doi.org/10.1074/jbc.RA118.005556.
15. Kreft SG, Hochstrasser M. 2011. An unusual transmembrane helix in the endoplasmic reticulum ubiquitin ligase Doa10 modulates degradation of its cognate E2 enzyme. J Biol Chem 286:20163–20174. https://doi.org/10.1074/jbc.M110.196360.
16. Mueller B, Klemm EJ, Spooner E, Claessen JH, Ploegh HL. 2008. SEL1L nucleates a protein complex required for dislocation of misfolded glycoproteins. Proc Natl Acad Sci U S A 105:12325–12330. https://doi.org/10.1073/pnas.0805371105.
17. Neuber O, Jarosch E, Volkwein C, Walter J, Sommer T. 2005. Ubx2 links the Cdc48 complex to ER-associated protein degradation. Nat Cell Biol 7:993–998. https://doi.org/10.1038/ncb1298.
18. Schuberth C, Buchberger A. 2005. Membrane-bound Ubx2 recruits Cdc48 to ubiquitin ligases and their substrates to ensure efficient ER-associated protein degradation. Nat Cell Biol 7:999–1006. https://doi.org/10.1038/ncb1299.
19. Langin G, Gouguet P, Üstün S. 2020. Microbial effector proteins—a journey through the proteolytic landscape. Trends Microbiol 28:523–535. https://doi.org/10.1016/j.tim.2020.02.010.
20. Price CTD, Al-Quadan T, Santic M, Rosenshine I, Abu Kwaik Y. 2011. Host proteasomal degradation generates amino acids essential for intracellular growth. Science 334:1553–1557. https://doi.org/10.1126/science.1212868.
21. Dorer MS, Kirton D, Bader JS, Isberg RR. 2006. RNA interference analysis of Legionella in Drosophila cells: exploitation of early secretory apparatus dynamics. PLoS Pathog 2:e34. https://doi.org/10.1371/journal.ppat.0020034.
22. Rodino KG, VieBrock L, Evans SM, Ge H, Richards AL, Carlyon JA. 2018. Orientia tsutsugamushi modulates endoplasmic reticulum-associated degradation to benefit its growth. Infect Immun 86:e00596-17. https://doi.org/10.1128/IAI.00596-17.
23. Myeni S, Child R, Ng TW, Kupko JJ, Wehrly TD, Porcella SF, Knodler LA, Celli J. 2013. Brucella modulates secretory trafficking via multiple type IV secretion effector proteins. PLoS Pathog 9:e1003556. https://doi.org/10.1371/journal.ppat.1003556.

24. Miller CN, Smith EP, Cundiff JA, Knodler LA, Bailey Blackburn J, Lupashin V, Celli J. 2017. A Brucella type IV effector targets the COG tethering complex to remodel host secretory traffic and promote intracellular replication. Cell Host Microbe 22:317–329.e7. https://doi.org/10.1016/j.chom.2017.07.017.
25. Borghesan E, Smith EP, Myeni S, Binder K, Knodler LA, Celli J. 2021. A Brucella effector modulates the Arf6-Rab8a GTPase cascade to promote intravacuolar replication. EMBO J 40:e107664. https://doi.org/10.15252/embj.2021107664.
26. Salcedo SP, Marchesini MI, Lelouard H, Fugier E, Jolly G, Balor S, Muller A, Lapaque N, Demaria O, Alexopoulou L, Comerci DJ, Ugalde RA, Pierre P, Gorvel J-P. 2008. Brucella control of dendritic cell maturation is dependent on the TIR-containing protein Btp1. PLoS Pathog 4:e21. https://doi.org/10.1371/journal.ppat.0040021.
27. Smith EP, Cotto-Rosario A, Borghesan E, Held K, Miller CN, Celli J. 2020. Epistatic interplay between type IV secretion effectors engages the small GTPase Rab2 in the Brucella intracellular cycle. mBio 11:e03350-19. https://doi.org/10.1128/mBio.03350-19.
28. Elbein AD, Tropea JE, Mitchell M, Kaushal GP. 1990. Kifunensine, a potent inhibitor of the glycoprotein processing mannosidase I. J Biol Chem 265:15599–15605. https://doi.org/10.1016/S0021-9258(18)55439-9.
29. Christianson JC, Shaler TA, Tyler RE, Kopito RR. 2008. OS-9 and GRP94 deliver mutant α1-antitrypsin to the Hrd1–SEL1L ubiquitin ligase complex for ERAD. Nat Cell Biol 10:272–282. https://doi.org/10.1038/ncb1689.
30. Hosokawa N, Wada I, Nagasawa K, Moriyama T, Okawa K, Nagata K. 2008. Human XTP3-B forms an endoplasmic reticulum quality control scaffold with the HRD1-SEL1L ubiquitin ligase complex and BiP. J Biol Chem 283:20914–20924. https://doi.org/10.1074/jbc.M709336200.
31. Hampton RY, Gardner RG, Rine J. 1996. Role of 26S proteasome and HRD genes in the degradation of 3-hydroxy-3-methylglutaryl-CoA reductase, an integral endoplasmic reticulum membrane protein. Mol Biol Cell 7:2029–2044. https://doi.org/10.1091/mbc.7.12.2029.
32. Grotzke JE, Lu Q, Cresswell P. 2013. Deglycosylation-dependent fluorescent proteins provide unique tools for the study of ER-associated degradation. Proc Natl Acad Sci U S A 110:3393–3398. https://doi.org/10.1073/pnas.1300328110.
33. Pizarro-Cerdá J, Méresse S, Parton RG, van der Goot G, Sola-Landa A, Lopez-Goñi I, Moreno E, Gorvel J-P. 1998. Brucella abortus transits through the autophagic pathway and replicates in the endoplasmic reticulum of nonprofessional phagocytes. Infect Immun 66:5711–5724. https://doi.org/10.1128/IAI.66.12.5711-5724.1998.
34. Celli J, Salcedo SP, Gorvel J-P. 2005. Brucella coopts the small GTPase Sar1 for intracellular replication. Proc Natl Acad Sci U S A 102:1673–1678. https://doi.org/10.1073/pnas.0406873102.
35. Swanson R, Locher M, Hochstrasser M. 2001. A conserved ubiquitin ligase of the nuclear envelope/endoplasmic reticulum that functions in both ER-associated and Matalpha2 repressor degradation. Genes Dev 15:2660–2674. https://doi.org/10.1101/gad.933301.
36. Taguchi Y, Imaoka K, Kataoka M, Uda A, Nakatsu D, Horii-Okazaki S, Kunishige R, Kano F, Murata M. 2015. Yip1A, a novel host factor for the activation of the IRE1 pathway of the unfolded protein response during Brucella infection. PLoS Pathog 11:e1004747. https://doi.org/10.1371/journal.ppat.1004747.
37. de Barsy M, Jamet A, Filopon D, Nicolas C, Laloux G, Rual J-F, Muller A, Twizere J-C, Nkengfac B, Vandenhaute J, Hill DE, Salcedo SP, Gorvel J-P, Letesson J-J, De Bolle X. 2011. Identification of a Brucella spp. secreted effector specifically interacting with human small GTPase Rab2: a Brucella effector interacting with Rab2. Cell Microbiol 13:1044–1058. https://doi.org/10.1111/j.1462-5822.2011.01601.x.
38. Döhmer PH, Valguarnera E, Czibener C, Ugalde JE. 2014. Identification of a type IV secretion substrate of Brucella abortus that participates in the early stages of intracellular survival: a novel Brucella virB secretion substrate. Cell Microbiol 16:396–410. https://doi.org/10.1111/cmi.12224.
39. Win J, Chaparro-Garcia A, Belhaj K, Saunders DGO, Yoshida K, Dong S, Schornack S, Zipfel C, Robatzek S, Hogenhout SA, Kamoun S. 2012. Effector biology of plant-associated organisms: concepts and perspectives. Cold Spring Harbor Symp Quant Biol 77:235–247. https://doi.org/10.1101/sqb.2012.77.015933.
40. Tanaka S, Brefort T, Neidig N, Djamei A, Kahnt J, Vermerris W, Koenig S, Feussner K, Feussner I, Kahmann R. 2014. A secreted Ustilago maydis effector promotes virulence by targeting anthocyanin biosynthesis in maize. eLife 3:e01355. https://doi.org/10.7554/eLife.01355.
41. Park C-H, Chen S, Shirsekar G, Zhou B, Khang CH, Songkumarn P, Afzal AJ, Ning Y, Wang R, Bellizzi M, Valent B, Wang G-L. 2012. The Magnaporthe oryzae effector AvrPiz-t targets the RING E3 ubiquitin ligase APIP6 to suppress pathogen-associated molecular pattern-triggered immunity in rice. Plant Cell 24:4748–4762. https://doi.org/10.1105/tpc.112.105429.
42. Ishikawa K, Yamaguchi K, Sakamoto K, Yoshimura S, Inoue K, Tsuge S, Kojima C, Kawasaki T. 2014. Bacterial effector modulation of host E3 ligase activity suppresses PAMP-triggered immunity in rice. Nat Commun 5:5430. https://doi.org/10.1038/ncomms6430.
43. Bos JIB, Armstrong MR, Gilroy EM, Boevink PC, Hein I, Taylor RM, Zhendong T, Engelhardt S, Vetukuri RR, Harrower B, Dixelius C, Bryan G, Sadanandom A, Whisson SC, Kamoun S, Birch PRJ. 2010. Phytophthora infestans effector AVR3a is essential for virulence and manipulates plant immunity by stabilizing host E3 ligase CMPG1. Proc Natl Acad Sci U S A 107:9909–9914. https://doi.org/10.1073/pnas.0914408107.
44. Chenon M, Camborde L, Cheminant S, Jupin I. 2012. A viral deubiquitylating enzyme targets viral RNA-dependent RNA polymerase and affects viral infectivity: TYMV DUB targets viral RdRp. EMBO J 31:741–753. https://doi.org/10.1038/emboj.2011.424.
45. Lombardi C, Ayach M, Beaurepaire L, Chenon M, Andreani J, Guerois R, Jupin I, Bressanelli S. 2013. A compact viral processing proteinase/ubiquitin hydrolase from the OTU family. PLoS Pathog 9:e1003560. https://doi.org/10.1371/journal.ppat.1003560.
46. Thiel H, Hleibieh K, Gilmer D, Varrelmann M. 2012. The P25 pathogenicity factor of beet necrotic yellow vein virus targets the sugar beet 26S proteasome involved in the induction of a hypersensitive resistance response via interaction with an F-box protein. Mol Plant Microbe Interact 25:1058–1072. https://doi.org/10.1094/MPMI-03-12-0057-R.
47. Jia Q, Liu N, Xie K, Dai Y, Han S, Zhao X, Qian L, Wang Y, Zhao J, Gorovits R, Xie D, Hong Y, Liu Y. 2016. CLCuMuB βC1 subverts ubiquitination by interacting with NbSKP1s to enhance Geminivirus infection in Nicotiana benthamiana. PLoS Pathog 12:e1005668. https://doi.org/10.1371/journal.ppat.1005668.
48. Chen P, Johnson P, Sommer T, Jentsch S, Hochstrasser M. 1993. Multiple ubiquitin-conjugating enzymes participate in the in vivo degradation of the yeast MATa2 repressor. Cell 74:357–369. https://doi.org/10.1016/0092-8674(93)90426-q.
49. Meyer HH, Shorter JG, Seemann J, Pappin D, Warren G. 2000. A complex of mammalian Ufd1 and Npl4 links the AAA-ATPase, p97, to ubiquitin and nuclear transport pathways. EMBO J 19:2181–2192. https://doi.org/10.1093/emboj/19.10.2181.
50. Mehrtash AB, Hochstrasser M. 2022. Elements of the ERAD ubiquitin ligase Doa10 regulating sequential poly-ubiquitylation of its targets. iScience 25:105351. https://doi.org/10.1016/j.isci.2022.105351.
51. Meyer H, van den Boom J. 2023. Targeting of client proteins to the VCP/p97/Cdc48 unfolding machine. Front Mol Biosci 10:1142989. https://doi.org/10.3389/fmolb.2023.1142989.
52. Schuberth C, Buchberger A. 2008. UBX domain proteins: major regulators of the AAA ATPase Cdc48/p97. Cell Mol Life Sci 65:2360–2371. https://doi.org/10.1007/s00018-008-8072-8.
53. Stevenson J, Huang EY, Olzmann JA. 2016. Endoplasmic reticulum-associated degradation and lipid homeostasis. Annu Rev Nutr 36:511–542. https://doi.org/10.1146/annurev-nutr-071715-051030.
54. Samanta D, Mulye M, Clemente TM, Justis AV, Gilk SD. 2017. Manipulation of host cholesterol by obligate intracellular bacteria. Front Cell Infect Microbiol 7:165. https://doi.org/10.3389/fcimb.2017.00165.
55. Foresti O, Ruggiano A, Hannibal-Bach HK, Ejsing CS, Carvalho P. 2013. Sterol homeostasis requires regulated degradation of squalene monooxygenase by the ubiquitin ligase Doa10/Teb4. eLife 2:e00953. https://doi.org/10.7554/eLife.00953.
56. Chua NK, Hart-Smith G, Brown AJ. 2019. Non-canonical ubiquitination of the cholesterol-regulated degron of squalene monooxygenase. J Biol Chem 294:8134–8147. https://doi.org/10.1074/jbc.RA119.007798.
57. Sharpe LJ, Howe V, Scott NA, Luu W, Phan L, Berk JM, Hochstrasser M, Brown AJ. 2019. Cholesterol increases protein levels of the E3 ligase MARCH6 and thereby stimulates protein degradation. J Biol Chem 294:2436–2448. https://doi.org/10.1074/jbc.RA118.005069.
58. Wang C-W, Lee S-C. 2012. The ubiquitin-like (UBX)-domain-containing protein Ubx2/Ubxd8 regulates lipid droplet homeostasis. J Cell Sci 125:2930–2939. https://doi.org/10.1242/jcs.100230.
59. Loregger A, Raaben M, Tan J, Scheij S, Moeton M, van den Berg M, Gelberg-Etel H, Stickel E, Roitelman J, Brummelkamp T, Zelcer N. 2017. Haploid mammalian genetic screen identifies UBXD8 as a key determinant of HMGCR degradation and cholesterol biosynthesis. Arterioscler Thromb Vasc Biol 37:2064–2074. https://doi.org/10.1161/ATVBAHA.117.310002.

60. Pereira-Dutra FS, Teixeira L, de Souza Costa MF, Bozza PT. 2019. Fat, fight, and beyond: the multiple roles of lipid droplets in infections and inflammation. J Leukoc Biol 106:563–580. https://doi.org/10.1002/JLB.4MR0119-035R.
61. Naroeni A, Porte F. 2002. Role of cholesterol and the ganglioside GM_1 in entry and short-term survival of Brucella suis in murine macrophages. Infect Immun 70:1640–1644. https://doi.org/10.1128/IAI.70.3.1640-1644.2002.
62. Watarai M, Makino S, Michikawa M, Yanagisawa K, Murakami S, Shirahata T. 2002. Macrophage plasma membrane cholesterol contributes to Brucella abortus infection of mice. Infect Immun 70:4818–4825. https://doi.org/10.1128/IAI.70.9.4818-4825.2002.
63. Smith EP, Miller CN, Child R, Cundiff JA, Celli J. 2016. Postreplication roles of the Brucella VirB type IV secretion system uncovered via conditional expression of the VirB11 ATPase. mBio 7:e01730-16. https://doi.org/10.1128/mBio.01730-16.
64. Xu Y, Liu Y, Lee J, Ye Y. 2013. A ubiquitin-like domain recruits an oligomeric chaperone to a retrotranslocation complex in endoplasmic reticulum-associated degradation. J Biol Chem 288:18068–18076. https://doi.org/10.1074/jbc.M112.449199.